https://doi.org/10.5194/ar-2026-24
Preprint. Discussion started: 30 June 2026

AEROSOL Research Discussions

Mixing state of Carbonaceous Aerosol Emissions from an Ecodesign Woodstove

Zixuan Cheng[1], Doğuşhan Kılıç [1,2], Daniel Wilson[3], Amanda Lea-Langton[3], Michael Flynn[1], Leonard Kirago[4,6], Marvin Shaw[4,5], Andrew Rickard[4,5], Jim R. Hopkins[4,5], Daniel Bryant[4,5], Gordon McFiggans[1], Jacqueline F. Hamilton[4,5], Hugh Coe[1,2] and James Allan[1,2*]

[1]Department of Earth and Environmental Sciences, The University of Manchester, Manchester, M13 9PL, UK

[2]National Centre for Atmospheric Science, The University of Manchester, Manchester, M13 9PL, UK

[3]Department of Civil Engineering and Management, The University of Manchester, Manchester, M13 9PL, UK

[4]Wolfson Atmospheric Chemistry Laboratories, Department of Chemistry, University of York, York, YO10 5DD, UK

[5]National Centre for Atmospheric Science, University of York, York, YO10 5DD, UK

[6]now at: African Research Centre on Air Quality and Climate, University of Mohammed VI Polytechnic, Ben Guerir, 43150, Morocco

[*]*Correspondence to: James Allan (James.Allan@manchester.ac.uk)*

Abstract

Residential wood burning (RWB) has become an increasingly significant source of carbonaceous aerosols (CAs) in the UK and worldwide. Black Carbon (BC) and Organic Aerosol (OA) fractions of CAs are of particular concern due to their impacts on climate and human health. Measuring the mixing state of CA is important as the mixing state can influence key aerosol properties including light absorption, hygroscopicity, cloud scavenging, atmospheric lifetime, and toxicity. While emissions and mixing states from traditional stoves have been previously reported and characterized, key uncertainties remain in the influence of user behaviour on emissions and the emission characteristics from the modern 'Ecodesign' appliances. Recent emissions tests imply that these can emit more pollutants such as polycyclic aromatic hydrocarbons (PAHs) and BC under certain circumstances and here we utilise online instrumentation to probe the mechanisms behind this and whether user behaviour has a role in impacting emissions. Hardwood logs were burned in a controlled test system using a UK Ecodesign-compliant woodstove under five operating protocols: standard, overload, underload, hot-reload and open-door protocols. Instantaneous particle emissions were quantified using a Single Particle Soot Photometer (SP2), a Differential Mobility Sizer (DMS500) and an Aerosols Mass Spectrometer (AMS). Modified combustion efficiency (MCE) was derived from CO and CO_2 concentrations measured by a Fourier-Transform Infrared (FTIR) spectrometer. Three typical combustion phases were observed: a pre-ignition phase, a flaming phase (with rich and non-rich flaming distinguished by an MCE of 0.95), and a smouldering phase. Stove operation can affect emissions by altering particle size, leading to ultrafine particle (UFP) formation (e.g., open-door, underload and overload conditions) and also prolong the rich flaming phase (e.g., hot-reload and overload), increasing PAH emissions. The findings here demonstrate how user behaviour may increase emissions of certain pollutants from modern stoves, partially offsetting the benefits compared to older designs.

https://doi.org/10.5194/ar-2026-24
Preprint. Discussion started: 30 June 2026

AEROSOL Research Discussions

1. Introduction

Particulate matter with diameter smaller than 2.5 micrometres ($PM_{2.5}$) is a significant health concern, which results in 4.2 million premature deaths annually (World Health Organisation, 2022). Residential wood burning (RWB) is a substantial contributor to both outdoor and indoor $PM_{2.5}$ emissions globally (Klimont et al., 2009; Cincinelli et al., 2019; Zhang et al., 2020; Font et al., 2022; Chowdhury et al., 2023). Black carbon (BC) and organic matter (OM), as significant fractions of PM emissions are carbonaceous materials produced through incomplete combustion, which have adverse human health effects including respiratory and cardiovascular diseases (Highwood and Kinnersley, 2006; Nichols et al., 2013).

BC is the dominant light-absorbing component of $PM_{2.5}$ and contributes to positive radiative forcing. Although its effective radiative forcing (from 1750 to 2019) is more than 10 folds lower compared with greenhouse gases (Szopa et al., 2021), the associated uncertainties remain large and may even reverse in sign. The uncertainties rise because BC remains inadequately represented in atmospheric models due to uncertainties in emissions, the complexity of simulating its microphysical and optical properties and its mixing state (Cappa et al., 2012; Liu et al., 2017). Freshly emitted BC typically exists as chain-like aggregates composed of primary spherules arranged in highly fractal geometries (Hu et al., 2021). These aggregates then re-agglomerate when mixed with other atmospheric components such as inorganic salts or OM (Wang et al., 2017). These mixtures can be either fully internal, meaning each particle homogeneously or heterogeneously contains all species, or fully external, meaning each particle contains only one species (Bond and Bergstrom, 2006). In practice, atmospheric BC particles typically exhibit a combination of internal and external mixing states due to atmosphere aging processes (Ye et al., 2018; Lee et al., 2019; Liu et al., 2020). OM is often co-emitted and mixed with BC, modifying the optical properties of BC-containing particles. For example, OM mixed with BC enhances light absorption by the particle through lensing effect when internally mixed, thereby influences BC radiative effects (Fuller et al., 1999; Bond et al., 2006; Liu et al., 2017; Ting et al., 2018; Yu et al., 2020).

The toxicity of OM, such as polycyclic aromatic hydrocarbons (PAHs), further increases human health risks when mixed with BC (Orasche et al., 2013). Under high concentrations, small particles (e.g., Aiken mode: 0.01μm – 0.1 μm) can coagulate with pre-existing particles to form larger particles (e.g., Accumulation mode: 0.1μm – 2.5 μm) (Liu et al., 2019; Yu et al., 2020). The particle coagulation rate is approximately proportional to the square of particle concentrations, consequently, BC particles can grow rapidly under high concentration conditions, for example in a wood stove (Ting et al., 2018).

RWB is estimated to contribute approximately 30% of the global BC emissions and 70% of the global OM emissions (Bond et al., 2004; Weimer et al., 2008; Klimont et al., 2017; Xu et al., 2021), with substantial regional variability caused by differences in stove design, fuel type, and user behaviour (Jetter et al., 2012; Bond et al., 2013). In the UK, surveys indicated that approximately 8% of households used solid fuels for space heating between 2015 and 2020 (Waters, 2016; Kantar, 2020). According to the UK National Atmospheric Emission Inventory (NAEI), RWB accounted for approximately 30% of the total $PM_{2.5}$ emissions in 2022, making it the dominant source in the UK (Mitchell et al., 2024), which decreased by 6.2% in 2023 compared to 2022. Observational data also support this reduction, likely attributable to the increased use of modern stove designs (Noonan et al., 2011; Font et al., 2022). For example, Ecodesign stoves include a secondary (and sometimes tertiary) air supply compared to traditional stoves, which can be preheated to deliver hot oxygen to the combustion zone which enhances combustion efficiency. Ecodesign stoves also feature thicker stove walls

https://doi.org/10.5194/ar-2026-24
Preprint. Discussion started: 30 June 2026

designed to reduce heat loss. However, non-ideal user behaviour during stove operation, such as using different sizes of logs, can alter PM emissions by up to 78% (Pettersson et al., 2011). Moreover, significantly higher PM emissions and PAH ratios have been reported when loading wood onto smouldering versus flaming embers (Pagels et al., 2013; Eriksson et al., 2014; Martinsson et al., 2015).

Ting et al. (2018) showed that the BC mixing state varies across combustion phases and exhibits certain relationship with modified combustion efficiency (MCE) in African cookstoves. A DEFRA (UK Department for Environment, Food and Rural Affairs) project (Allan et al., 2024a) lead by Ricardo Plc. developed a standard stove testing protocol informed by a DEFRA burning survey data. The protocol was developed and adapted for different stoves in response to challenges and findings from combustion experiments, for the purposes of informing the NAEI (Allan et al., 2024b; Allan et al., 2025). Traditional stoves and modern stoves were tested in DEFRA project using commonly used fuels (e.g., wood logs with different moisture content, mineral fuels). DEFRA project showed that modern stoves, including Ecodesign and Blue-Sky-Angel stoves, exhibited higher emissions of CO, PM, volatile organic compounds (VOCs) and PAHs when burning dry wood compared to traditional designed stoves. Nevertheless, there are several open scientific questions remaining on the emissions from Ecodesign wood stoves: (1) how deviations (e.g., fuel types, refuelling timing, operations) from the standard test protocol influence BC mixing states and online stove emission characterisation; (2) which parameters and microphysical processes govern the CA emissions; (3) what mechanisms lead to increased BC and PAHs emissions when burning dry wood in modern stoves.

Emissions from non-ideal stove operation are often only partially accounted or completely omitted in RWB emission factors and activity data used in inventories, highlighting the necessity for targeted research on stove emissions (Allan et al., 2024b; Elliott et al., 2025). Given the need to answer these important science questions the "CondensabLe AeRosol from non-Ideal Stove Emissions" (CLARISE) project aims to investigate stove emissions under non-ideal operational conditions including non-ideal user behaviour and unconventional fuels. This study aims to quantify and characterize primary BC and OM emissions from non-ideal stove operation of an Ecodesign woodstove in a comprehensive set of laboratory experiments using high-resolution online instruments, including a single particle soot photometer (SP2, DMT) and an aerosol mass spectrometer (AMS, Aerodyne). BC concentrations and mixing states were quantified and characterized using the incandescence and scattering channels of the SP2. OM concentrations and chemical composition were measured using an AMS. A differential mobility sizer (DMS500) and a fourier-transform infrared spectrometer (FTIR GT6000, Gasmet) were used to characterize flue emissions.

2. Experimental

2.1 Condensable Aerosol from non-Ideal Stove Emissions project

2.1.1 Experimental setup

Figure 1 presents the CLARISE instrumentation and flow configuration. A temperature sensor to measure the flow and ember temperature. A fourier-transform infrared spectrometer (FTIR, Gasmet) and a DMS500 (Cambustion) were deployed to characterize flue emissions, providing gas phase composition and particle size

https://doi.org/10.5194/ar-2026-24
Preprint. Discussion started: 30 June 2026

distributions. The flow was initially diluted with a nose-cone stove flue adaptor and was subsequently diluted using a ejector dilutor (Dekati). Diluted primary emissions were then measured using a high-resolution AMS (Canagaratna et al., 2007; Haslett et al., 2018) and an SP2 to measure refractory black carbon (rBC) mass concentrations(Liu et al., 2019; Cheng et al., 2025). The flow could also be aged in an oxidation chamber if switched to secondary. The flow can be measured using the same suite of online instruments after aging in the chamber. A four way valve enabled switching between the secondary and primary sampling lines. As this paper aims to quantiying primary emission, the chamber analysis will be presented in a future publication. Therefore, the chamber data were removed from all other analysis except time series.

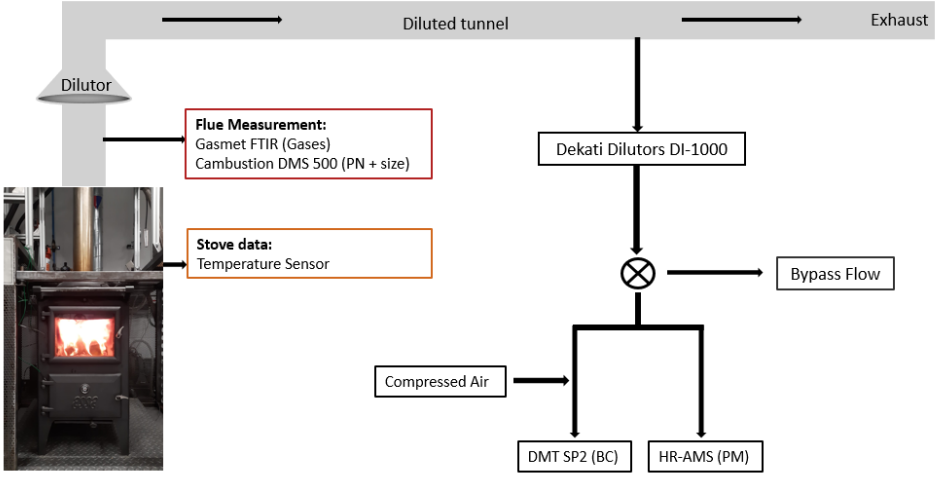

Figure 1 Schematic diagram of the experimental setup used in the CLARISE. Flue emissions were first measured by an FTIR and a DMS500 to determine gas composition and particle size distributions. The flow was then first diluted at the stove outlet tunnel by a nose-cone flue adaptor and was further diluted with a Static Ejector Dilutor. The diluted flow was directed to online instruments.

2.1.2 Manchester stove facility

The Manchester stove facility operates an Ecodesign compliant multifuel stove (50 x 60 x 90 cm, ESSE Bake Heart), equipped with a cooking pan on the top and an oven at the bottom (Fig. 1), which is a widely used cookstove across the UK. This Ecodesign stove has two independent air supplies (i) from underneath (1st supply) and (ii) from the back (2nd supply) of the stove. The pre-heated secondary air delivers additional hot oxygen to the combustion zone, increasing the combustion efficiency. Under real-world operating conditions, the exhaust stream passes through a catalyst and is then vented via the flue. To characterize the emissions, we removed the catalyst during the experiments.

https://doi.org/10.5194/ar-2026-24
Preprint. Discussion started: 30 June 2026

2.1.3 Standard protocol - Fuel

The standard CLARISE protocol follows the same procedures as outlined in the DEFRA stove testing protocol (Allan et al., 2024a). Logs from various species (Ash, Beech and Pine) and manufactured wood products such as construction off-cuts and commercially available fire logs were selected as laboratory test fuels because they are widely used across the UK. Logs were cut to 35-38 cm in length and 5-10 cm in diameter, debarked, and trimmed to a nominal mass of 700 g. Manufactured wood logs were similarly cut to achieve a target mass of 700 g. The moisture content of the wood logs used was very low at < 6%. To achieve this moisture, the wood was conditioned in an air-conditioned laboratory for an extended period prior to the experiments. Moisture content was measured using a calibrated moisture meter before loading the logs in the stove. In the data presented here, dry Ash logs were used for all experiments.

2.1.4 Standard protocol – Burn cycle

Kindling fires (start-up from a cold stove) were initiated using small pieces of Ashwood with a total mass of 350 g. During ignition, the air inlet was fully opened and the secondary inlet set to 75%. Two commercial firelighters and a propane torch were used to ignite the kindling. After lighting the kindling wood, the stove door was kept ajar by about 2 cm for 3 minutes until the flames had become established, then the door was fully closed.

During the burning, the tunnel flow was adjusted to maintain the flue exit at 800 feet per minute (FPM); measured by a Dwyer 460 Air Meter Kit). When flames from a load (kindling or logs) subsided, the embers were shovelled flat and two new 700 g logs were added to the firebox (Allan et al., 2024b; Allan et al., 2024a; Allan et al., 2025). This refuelling initiated a new log burn cycle. The kindling phase was excluded from cycle analysis because its geometry was not reproducible, all burn cycle statistics therefore refer to the log cycle.

2.1.5 Stove operations

Non-ideal operation refers to deviations from the standard protocol during refuelling onto an ember bed and/or subsequent burn cycle, all other operating variables follow the standard protocol. To assess how user behaviour alters stove emissions, five non-ideal operating protocols were designed: “Overload”, “Underload”, “Open-door”, “Single big log”, and “Hot reload”. Each protocols reflects plausible real-world constraints and preferences.

1. **Overload**: the burn cycle starts with four logs (700 g each) instead of two. Users overload to reduce the frequency of loading for convenience and improve the efficiency of heating the stove for gaining more heat.
2. **Under-load**: the burn cycle starts with a single wood log (700 g). Underload provided a contrast to the Overload protocol.
3. **Single big log**: the burn cycle starts with one large log (1400 g). This protocol reflected real world variability in fuel size and examined its effect on stove emissions.
4. **Open-door**: the burn cycle starts with the stove door left ajar about 2 cm throughout the whole burning cycle (two logs, 700 g each). Users keep door open to accelerate ignition of dense or moist fuel, to

https://doi.org/10.5194/ar-2026-24
Preprint. Discussion started: 30 June 2026

mitigate perceived smoke spillage during reloading, or a belief that additional air from front door improves combustion efficiency.

5. **Hot-reload**: two new wood logs (700 g each) are loaded onto glowing embers while a residual flame is still present (before flame extinction). Hot loading is employed to maintain continuous flame for space heating (thermal comfort) or cooking and to avoid the effort of re-lighting. A hot-reload protocol was used as the laboratory method for continuous combustion emission measurements (Eriksson et al., 2014).

Top-down ignition was tested as an alternative cold start procedure. Two 700 g logs were placed at the bottom of the firebox, followed by 350 g of kindling wood pieces and two commercial firelighters above logs. The firelighters were ignited so that combustion proceed from the top of the fuel stack downward. The primary and secondary air setting, ignition operation, and dilution tunnel flow were the same as the standard protocol. Top-down ignition was included in this study because it has been recommended as a low-emission startup practice (United Nations Economic Commission for Europe, 2021) and has been shown to reduce startup emissions comparing to conventional bottom-up ignition (Brandelet et al., 2018).

2.2 Instrumentation

Table 1 Measurement instruments used in this study, including instrument names, measurement frequency, measured and derived parameters.

Instrument	Time resolution	Measured parameters*	Derived parameters*
SP2	1 s	rBC Concentrations D_c D_p	D_p/D_c CMD MMD E_{sca} F_{in}
AMS	30 s	OM Mass Concentrations Mass Spectra	*m/z* 60, *m/z* 202 Organic Fraction F_{in}
DMS500	0.1 s	Electromobility Distributions	Number Concentrations D_m
FTIR	30 s	Flue CO, CO_2 Concentrations	MCE
LI-COR	1 s	Bypass CO_2 Concentrations	Dilution Factor

*Note: rBC concentrations: number and mass concentrations, D_c: rBC core diameter, D_p: BC particle diameter, CMD: rBC core count median diameter, MMD: rBC core mass median diameter, E_{sca}: scattering enhancement, F_{in}: internally mixing factor, *m/z*: the mass-to-charge ratios of organic marker ions detected by AMS, D_m: particle size as mobility diameter, MCE: modified combustion efficiency.

2.2.1 Single Particle Soot Photometer

Particle size and mixing state of individual BC and mass concentrations of rBC were measured using an SP2 which uses the laser induced incandescence technique (Schwarz et al., 2006; Gao et al., 2007; Liu et al., 2014; Michelsen et al., 2015). The SP2 measurement principle, calibration procedure and data retrieving have been described in detail elsewhere (Liu et al., 2014; Liu et al., 2019; Yu et al., 2020; Cheng et al., 2025). In this study, the mass-equivalent diameter of rBC core (D_c) is determined from the measured rBC mass by assuming a BC density of 1.8 g cm^{-3} (Bond and Bergstrom, 2006).

https://doi.org/10.5194/ar-2026-24
Preprint. Discussion started: 30 June 2026

AEROSOL Research Discussions

The scattering signal of BC containing particles measured by the SP2 is determined using a leading edge only (LEO) technique, which is a reconstruction of distorted scattering signal when particle passes through laser beam and heated (Gao et al., 2007). This allows to determine the diameter of BC particles (D_p) after matching scattering signal with LEO fitted to a Mie core-shell lookup table (Taylor et al., 2015). Therefore, the bulk relative coating thickness (D_p/D_c) of BC particles is determined to indicate the coating (Liu et al., 2014):

$$\frac{D_p}{D_c} = \sqrt[3]{\frac{\sum_i D_{p,i}^3}{\sum_i D_{c,i}^3}}, \quad (1)$$

Where $D_{p,i}$ and $D_{c,i}$ are the D_p and D_c of each BC particles. For a time interval, averaged D_c can be reported as mass median diameter (MMD). The distribution of coating thickness on D_c range can be further investigated by Scattering Enhancement (E_{sca}) which is defined as the ratio of the measured scattering signals of a rBC containing particle after LEO fitting, to the calculated scattering intensity for the uncoated BC core inside the particle (Liu et al., 2014):

$$E_{sca} = \frac{S_{measured,BC\ particle}}{S_{calculated,BC\ core}}, \quad (2)$$

Where $S_{measured,BC\ particle}$ is the scattering intensity of a rBC-containing particle measured by SP2 after LEO fitting. $S_{calculated,BC\ core}$ is the scattering intensity of the corresponding rBC core calculated using the measured rBC mass and BC refractive index (2.26 + 1.26i) at 1064 nm (Moteki et al., 2010). For the determination of E_{sca} and D_p/D_c, the value of E_{sca} = 1 and D_p/D_c =1 indicate bare rBC particle, because any non-rBC material coated on the BC core will enhance the light scattering. However, due to instrumental and methodological uncertainties, values of E_{sca} < 1 can occur (Liu et al., 2014; Liu et al., 2017; Liu et al., 2019). Nevertheless, E_{sca} is a useful indicator to investigate BC mixing states.

SP2 had additional coincidence when measuring sample flow with high concentration (Schwarz et al., 2006). In this study, we introduced an additional dilution by adding 75 ccm compressed air, controlled by a flow meter (Alicat Scientific, Inc.), after ejector dilutor (prior to the SP2 inlet).

2.2.2 High Resolution Aerosol Mass Spectrometer

High resolution AMS (Aerodyne) was used here to measure non-refractory aerosol chemical compositions by fractionating sulfate, nitrate, ammonium, chloride and organic aerosols online. The operational and data analysis procedures for AMS have been described elsewhere (Canagaratna et al., 2007; Hu et al., 2023). The AMS was operating with flow rate of 0.10 L min^{-1}, and the ionization efficiency was calibrated using monodisperse ammonium nitrate particles. Mass concentrations of organic marker ions (e.g., ions at mass-to-charge ratios *m/z* 60 and 202) were derived from AMS mass spectra, and organic fractions were calculated relative to the total organic aerosol mass concentrations.

Previous studies (Haslett et al., 2018; Hu et al., 2021) reported mass spectra from highly controlled measurements of aerosols emissions from commonly used wood (Africa and UK) using combustion hoods. Here, we extend this work by presenting detailed mass spectra (including PAHs) from Ecodesign stove operated under different protocols.

https://doi.org/10.5194/ar-2026-24
Preprint. Discussion started: 30 June 2026

2.2.3 Fourier Transform Infrared Spectrometer

FTIR (GT6000; Gasmet, Finland) measured the concentrations of CO and CO_2 at the flue. Daily procedures included zero calibration using nitrogen and filter cleaning with acetone in an ultrasonic bath.

2.2.4 Differential Mobility Spectrometer

The DMS500 (Cambustion Ltd., Cambridge, UK) (Reavell et al., 2002; Symonds et al., 2007) measured particle size distributions and number concentrations using electrical aerosol spectrometer (Mirme et al., 1984). Aerosol sizes from 5 nm to 2.5 µm can be measured by DMS500 at 10 Hz time resolution, with an 8 L min^{-1} flow rate, after being charged by a controlled corona charger designed to minimise diffusion losses. In this study, soot calibration was performed using a bimodal agglomerates to reinvert the data (Symonds et al., 2007) as the flaming phase particles are soot like (Hu et al., 2021). The morphology of the nucleation mode particles during pre-ignition and smouldering is uncertain and may be spherical which leads to uncertainties when estimating the concentration using agglomerates calibration. Nevertheless, alternative calibrations shifted the nucleation mode particle peaks only slightly here, indicating that particle shape has limited impact on their electrical mobility. The bimodal agglomerates calibration is therefore considered robust here. The particle size diameter measured by DMS500 is reported as mobility diameter (D_m) hereafter.

2.2.5 Non-Dispersive Infrared gas analyzer

Carbon dioxide (CO_2) concentrations before the bypass were measured by an infrared gas analyser (Li-Cor LI – 820; Lincoln, NE, USA), which is an infrared gas analyzer (IRGA), with 1 Hz time resolution and a flow rate of 1 L min^{-1} flow rate. Daily procedures included zero calibration of the analyser using nitrogen.

2.2.6 Dilutor

Flue sample was further diluted using an ejector dilutor (Dekati Diluter DI-1000; Finland), in which high speed compressed air flows into an ejector nozzle and causes a pressure drop which draws the sample flow into the dilutor through the nozzle. The sample flow is instantaneously diluted as it mixes with compressed air.

2.3 Data processes

2.3.1 Dilution factor and modified combustion efficiency

The dilution factor in CLARISE experiments were calculated as 58 ± 7 using CO_2 measurements from FTIR and LI-820 from near the initial flue and bypass, respectively.

MCE is commonly used to identify burn phase boundaries. MCE is calculated as the ratio of emitted CO_2 to the sum of CO_2 and CO (Eriksson et al., 2014; Haslett et al., 2018; Ting et al., 2018):

$$\mathrm{MCE} = \frac{\Delta CO_2}{\Delta CO_2 + \Delta CO}, \quad (3)$$

https://doi.org/10.5194/ar-2026-24
Preprint. Discussion started: 30 June 2026

AEROSOL Research Discussions

where CO and CO_2 concentrations were measured by FTIR. This calculation provides the percentage of carbon release by CO_2 by assuming PM, other gas-phase organic compounds, methane (CH_4) and other larger molecules contributes negligibly (around 4%) (Mcmeeking et al., 2009; Haslett et al., 2018).

2.3.2 Internal mixing factor

To better understand the internal and external mixing of BC and OM, an internal mixing factor (F_{in}) was determined using OM and rBC concentrations measured by AMS and SP2 following the same approach as (Ting et al., 2018) to allow comparison across different stove types:

$$F_{in} = \frac{\left[\left(\frac{D_p}{D_c}\right)^3 - 1\right] \times \frac{\rho_{OM}}{\rho_{rBC}} \times \sum_i rBC_i}{OM_{total}}, \quad (4)$$

where $\frac{D_p}{D_c}$ is BC coating bulk determined in Eq. (1). ρ_{OM} and ρ_{rBC} are the density of OM and BC assumed to be 1.2 g cm^{-3} and 1.8 g cm^{-3} respectively. $\sum_i rBC_i$ is the total mass of rBC measured by SP2. OM_{total} is the total OM measured by the AMS. F_{in} can produce a good estimation of BC and OM mixing state even with minor uncertainties due to SP2 detection limit (< 70 nm) (Ting et al., 2018).

3. Results and Discussion

3.1 High resolution burning cycles

Figure 2 presents an exemplar measurement time series from a standard CLARISE burn protocol, including rBC, OM, the OM fraction (OM/OM+BC), pyrene (*m/z* = 202), levoglucosan (*m/z* = 60), BC core size, BC coating bulk, flow temperature and MCE. The OM/(OM+BC) ratio is commonly used to identify the combustion phase. Pyrene is the most prominent of the PAH peaks observed in the AMS, consistent with Eriksson et al. (2014), and is used as a marker for these. A high ratio indicates OM is the dominant fraction among aerosols emitted while a lower ratio indicates BC is the dominant aerosols. The highest OM fraction (ratio > 0.5) was observed during the kindling and ignition phases. This ratio decreased with the start of flaming (Fig. 2 d). Kindling emissions were not widely reported in previous studies owing to poor repeatability (Eriksson et al., 2014). However, kindling at lower temperatures (< 150 °C approximately), by reducing MCE, can increase RWB emissions especially OM emissions (Fig. 2). As shown in Fig. 2, ignition of the firelighters leads to an immediate increase in rBC, driven both by the firelighter flame and charring of the overlying kindling. Once the kindling woods were ignited, rBC concentrations decreased whereas OM emissions increased. MCE also decrease during this “cold-start” ignition phase, indicating incomplete combustion due to the low temperature. The pattern of the OM/(OM+BC) seen is observed in most of the burn experiments; however, time series pattern of the OM and BC particle concentrations were highly variable during pre-ignition and the start of the ignition although using the same amount of kindling wood.

https://doi.org/10.5194/ar-2026-24
Preprint. Discussion started: 30 June 2026

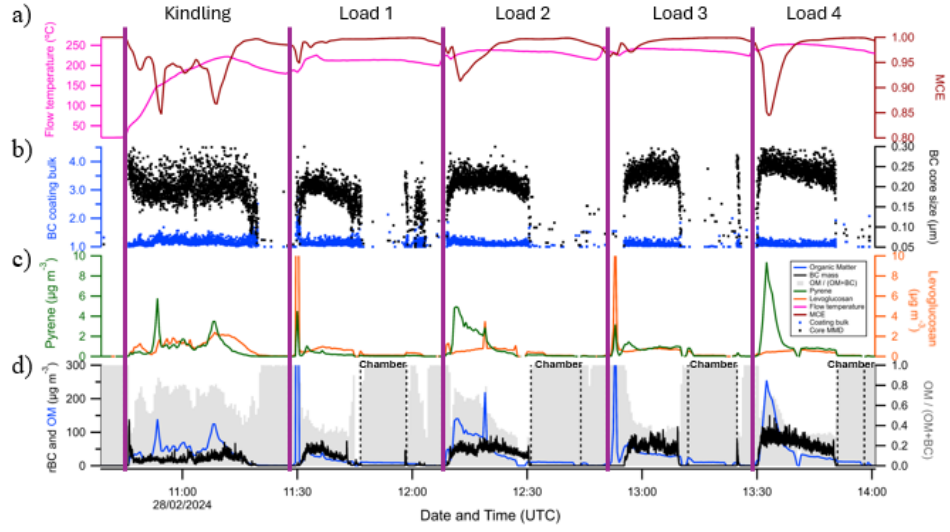

Figure 2 Time series of OM, rBC, OM fraction (OM/OM+BC), pyrene, levoglucosan, BC core size and BC coating bulk for a standard burn experiment. Temperature and Modified Combustion Efficiency (MCE) are included to identify combustion conditions. Four test burns including one kindling at the beginning are shown.

During each burn cycle, OM emissions increased immediately after putting logs on the kindling embers and before logs were ignited, marking the pre-ignition phase which is driven by the pyrolysis of the wood. Levoglucosan concentration, measured by AMS at *m/z* 60 (Fig. 3 c), served as a marker for this pre-ignition/pyrolysis phase (also shown in Fig. 2 for additional burn cycles). The high emissions of OM likely originated from the surface or near surface layers of the wood undergo pyrolysis on the hot embers. These pyrolysis OM products can be present in both particle- and gas-phase, by either condensing or coagulating with each other in the cooling mixture of emissions (Haslett et al., 2018). However, deviations were sometimes observed, for example, the pre-ignition phase was short in load 2 and not obvious in load 4 (Fig. 2). In load 2, the two logs were placed close to each other, which may have inhibited pyrolysis by charring or combustion of released volatiles in the confined gap. In load 4, higher ember temperature led to rapid ignition, likely efficiently burning volatile pyrolysis products in flames, forming higher rBC and PAHs (e.g., pyrene) but lower levoglucosan. The decrease in MCE during pre-ignition suggests incomplete combustion due to limited oxygen under fuel-rich conditions (Ting et al., 2018), which may intensify when loading onto hot or even glowing embers (see supplementary material Fig. S15) (Eriksson et al., 2014). During these pre-ignition phases, rBC concentrations were relatively low as BC formation is primarily linked to flaming combustion.

After the pre-ignition phase, OM concentrations immediately decreased. Upon ignition, both OM and rBC increased rapidly, reached peak (diluted) concentrations of approximately 50 µg m^{-3} and 75 µg m^{-3}, respectively. This OM and BC rise was accompanied by a decrease in the OM/(OM+BC) ratio, indicating a transition into flaming phase, which was widely observed before (Eriksson et al., 2014; Haslett et al., 2018; Ting et al., 2018). During flaming phase, MCE can efficiently and quantitatively indicate the burning efficiency conditions. Following Ting et al. (2018), we classified flaming phase into non-rich (MCE > 0.95) and rich (MCE < 0.95). When rBC concentrations stabilized around 50 µg m^{-3} and the OM/(OM+BC) was low (around 0.7), it suggested

https://doi.org/10.5194/ar-2026-24
Preprint. Discussion started: 30 June 2026

a stable flame regime. Rich flaming was characterized by increased CO concentration, oxygen deficiency, low flue temperatures and enhanced OM emissions, including Pyrene, consistent with previous observations (Eriksson et al., 2014; Ting et al., 2018). For example, in a standard load shown in Fig. 3, the averaged CO concentration reached 4628 ppm during rich flaming, approximately 11 times higher than during non-rich flaming. OM concentrations exceeded 100 μg m^{-3}, while pyrene exceeded 3 μg m^{-3}. This indicates rich flaming, arising when available combustible gases exceed the oxygen levels, thereby limiting oxidation and promoting incomplete combustion. An exemplar rich flaming time series is available in Fig. S15. Throughout the non-rich flaming phase, MCE remained consistently above 0.99 (table 2), which is slightly higher than open burning (above 0.98) (Haslett et al., 2018) and pre-Ecodesign stoves (approximately 0.95 - 0.98) (Ting et al., 2018). This MCE behaviour is expected because the Ecodesign stove supplies preheated secondary air that promotes complete combustion. Short-lived OM and levoglucosan spikes were measured during flaming associated with the mechanical breakup of the log (Fig. 3, wood crack). These short-lived spikes may indicate pyrolysis occurring in the cooler core of the log. Pyrolysis products can be trapped in the charr layer because the charring surface has low thermal conductivity (Haslett et al., 2018). When the wood cracks and splits during flaming, these products may be released to flue as a plume if not consumed by the flames.

Approximately 13 minutes after ignition, rBC concentrations decreased below the detection limit, therefore the OM/(OM+BC) ratio increased sharply, indicating a transition to the smouldering phase (Fig. 3). Smouldering phase is characterized by the absence of visible flames, leading to minimal rBC formation. OM concentrations were also decreased due to fuel depletion. Smouldering phase is thus a relatively “clean” combustion phase in terms of BC emissions. Towards the end of the smouldering phase, MCE decreased again (smouldering rich), likely due to oxygen-limited conditions caused by tightly packed embers, which hinder air diffusion and suppress complete combustion. However, limited fuel availability constrained BC formation, resulting in low BC concentrations.

Previous studies often use MCE to define burning phases. However, as pointed out by Ting et al. (2018), MCE provides an incomplete descripton, as pre-ignition processes are not captured by combustion-based metrics. Consequently, the decreases in MCE observed during pre-ignition and smouldering (Fig. 3) do not provide a clear threshold for distinguishing pre-ignition from flaming combustion. In this study, we used a combination of particle size distribution data (Fig. S2) and OM/(OM+BC) ratio to identify pre-ignition, flaming and smouldering phases, while reserving MCE = 0.95 to distinguish between rich and non-rich flaming within the flaming phase.

https://doi.org/10.5194/ar-2026-24
Preprint. Discussion started: 30 June 2026

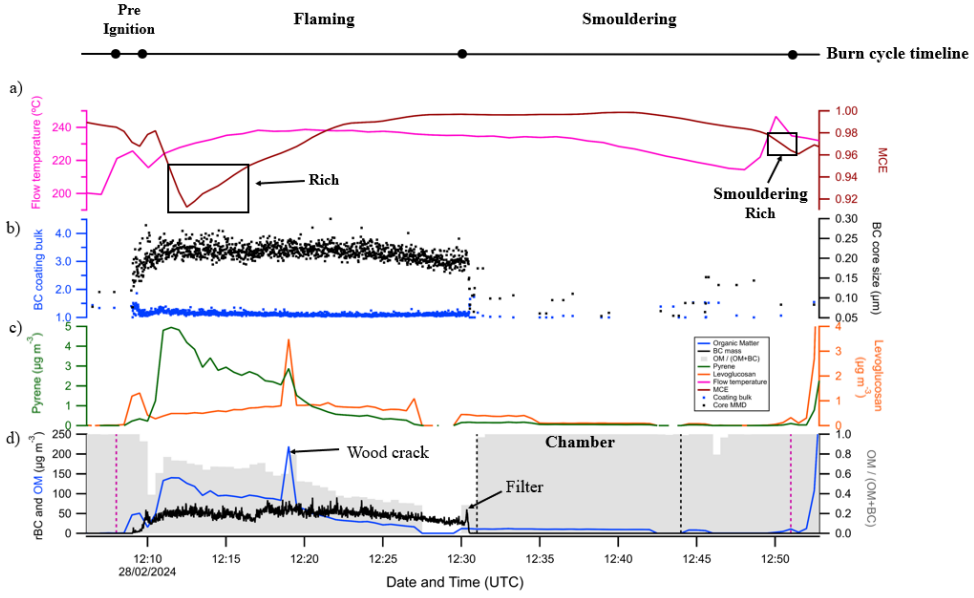

Figure 3 Temporal evolution of a standard burn cycle. Panel a) shows the time series of the sample flow temperature and MCE; panel b) is the time series of the bulk BC coating and BC core size; panel c) shows the time series of pyrene and levoglucosan concentrations; panel d) is the time series of rBC, OM and OM/(OM+BC) ratio. Vertical dashed purple lines mark the start and end of the burn cycle, while vertical dashed black lines indicate chamber (aging) sampling periods which were excluded in this study. Wood crack and filter procedure are annotated. Periods of rich flaming (low MCE periods, shown on panel a) and rich smouldering are identified and annotated in the MCE panel (panel a).

3.2 Mass spectra of OM

Mass spectra of aerosol emissions from the Ecodesign stove operated under different combustion protocols, together with differential mass spectra for different burn phases, are presented in Fig. S10 – S14 and Fig. 4, including detailed PAH signatures. These measurements complement earlier laboratory studies based on combustion hoods

Non-rich flaming was selected as the reference phase because it exhibited relatively stable and low OM production, allowing phase-specific emissions during other combustion phases to be more clearly identified (Fig. 4). Pre-ignition and smouldering mass spectra were dominated by hydrocarbon ion fragments including C_nH_{2n-1} (*m/z* 55) and C_nH_{2n+1} (*m/z* 29, 43, 57) (Fig. 4 a, c). However, PAHs including $C_{16}H_{10}$ (*m/z* 202), $C_{18}H_{10}$ (*m/z* 226) and $C_{20}H_{12}$ (*m/z* 252) were also observed during both rich and non-rich flaming conditions while rich flaming produced higher concentrations and additional compounds such as $C_{18}H_{12}$ (*m/z* 228), $C_{20}H_{10}$ (*m/z* 250) and $C_{22}H_{12}$ (*m/z* 276) (Fig. 4 b). The Ecodesign stove produce more PAHs when burning drywood (Allan et al., 2025), here we found that these PAHs are mainly produced due to rich flaming. PAH emissions from wood burning strongly depend on the release of volatile organics during pyrolysis (Lea-Langton et al., 2019), a process that progresses from the wood surface towards the interior over the course of the burning cycle. The Ecodesign stove may enhance pyrolysis because the secondary air can locally cool the firebox, which may explain lower PAH emissions observed in more traditional stoves. Pre-ignition phase may efficiently release the

https://doi.org/10.5194/ar-2026-24
Preprint. Discussion started: 30 June 2026

VOCs before flaming. This may explain higher PAH content and longer rich flaming period during hot reload burns (Fig. S7, Table 2), because hot-reloads typically has a very short (or no detectable) pre-ignition phase. By contrast, pre-ignition phase was longer under the single big log protocol with little to no rich flaming observed (Fig. S6).

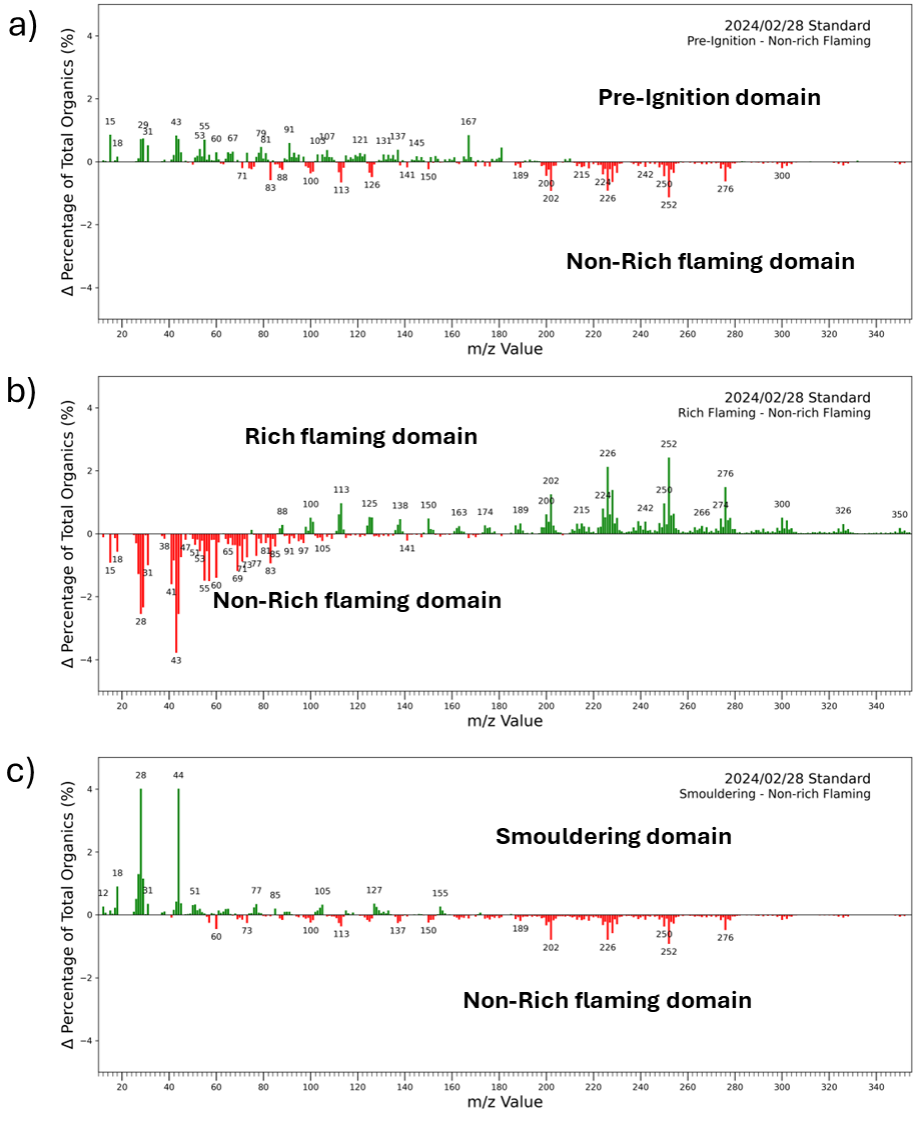

Figure 4 Comparison of organic aerosol composition using averaged mass spectra for a) pre-ignition and b) rich flaming and c) smouldering phases, all relative to the non-rich flaming as the reference case.

Pre-ignition and smouldering produced less PAHs than flaming but produced small OA fragments. Prominent pre-ignition organic peaks included *m/z* 55, 60, 73, 91, 137, 167. Pre-ignition peaks at *m/z* 60 and 137 are attributed to levoglucosan (Fig. 4 a). These peaks were unique to the pre-ignition phase (among all phases) and

https://doi.org/10.5194/ar-2026-24
Preprint. Discussion started: 30 June 2026

may serve as a marker of pyrolysis. Peaks at *m/z* 167 and 181 have previously been strongly associated with biomass (Alfarra et al., 2007; Weimer et al., 2008) and incense burning (Li et al., 2012). In this study (Fig. 4 a), the peak at *m/z* 167 could be linked to lignin-related compounds which are relatively more resistant to thermal decomposition during the pre-ignition phase. During smouldering, prominent organic peaks included *m/z* 44 and 28. The *m/z* 44 peak (CO_2^+) which may be originating from $C_2H_4O^+$, which is also probably from lignin and may be the last remaining compound to thermally decompose therefore the peak is detected during smouldering phase (Hu et al., 2021). The CO_2^+ (*m/z* 44) and CO^+(*m/z* 28) peaks can also originate from nitrate and ammonium salt (e.g., NH_4NO_3) in the AMS (Pieber et al., 2016; Mărmureanu et al., 2025). The biases, related to interference from inorganic salts contributing falsely to the organic signal, varied across instruments and become significant when measuring aerosols with low organic but high inorganic fractions. Pre-ignition produced larger compounds than smouldering (Fig. 4 a, c), consistent with previous studies (Haslett et al., 2018). DMS500 size distribution data (Sect. 3.3.2) further show that smouldering mainly produced smaller particles, consistent with the studies described above.

Non-ideal operations can shorten or extend combustion phase durations, for example, hot reload and overload extended rich flaming phase duration (Table 2), but the aerosol chemical composition did not significantly change across protocols (Fig. S4 – S9). However, the open-door burn represents an exception, as rich flaming was associated with comparatively low PAH emissions (Fig. S8 d), likely due to increased air flow from front door limited the residence time of VOCs and local cooling prevented PAH formation.

3.3 Carbonaceous aerosols mixing state

3.3.1 BC mixing state

Figure 5 presents the BC core diameter and E_{sca} values for six burn protocols, the particle number densities exceeding 70% of the total are shown in red. Some BC particles were observed with a scattering enhancement below one ($E_{sca} < 1$), attributed to minor scattering channel miscalibration and to deviations from Mie theory assumptions: uncoated or very thinly coated BC cores can scatter less light than predicted by the model, which assumes these are spherical particles in a homogeneous refractive index. In addition, the refractive index (RI) of biomass burning aerosols can be different from traffic related aerosols (Liu et al., 2019), further influencing the optical calculations. For clarity of reporting, a scattering enhancement factor less than 1 ($E_{sca} < 1$) was assumed to indicate effectively uncoated BC particles .

During the standard, open-door, overload and hot-reload burn protocols (Fig. 5 a, b, e, f), BC particles exhibited a clear resolved bimodal E_{sca} distribution, with one mode close to $E_{sca} \approx 1$ and a second mode at higher E_{sca}. By comparison, the underload and single big log burn protocols (Fig. 5 c, d) still showed two BC particle populations, but the separation between them was much weaker, producing a more continuous, near monomodal E_{sca} distribution. The clear resolved bimodal BC mixing pattern comprises (i) uncoated BC across a broad size range and (ii) a thickly coated group with $E_{sca} > 1$. E_{sca} values in the thickly coated group occasionally exceed 10. These physically distinct BC types likely reflect flame heterogeneity. Because the bimodal pattern occurred across several protocols, it appears intrinsic to the burn cycle itself and may be controlled by fluctuations in MCE rather than being protocol specific.

https://doi.org/10.5194/ar-2026-24
Preprint. Discussion started: 30 June 2026

In contrast, the bimodal pattern was not obvious under underload (Fig. 5 c) and single big log (Fig. 5 d) protocols. We attributed this discrepancy to sufficient oxygen availability at the reduced combustion surface, which may accelerate oxidation of volatile pyrolysis products and suppresses their condensation onto BC cores. BC mixing state varied across burn protocols, indicating the important of accurate source apportionment at measurement site affected by wood burning plumes, as wood burning can also produce thinly coated BC resembling traffic emissions (Liu et al., 2014; Liu et al., 2019). The typical thickly coated ambient wood burning BC were observed in London and Beijing but were not observed in this study (Fig. 5). As discussed above, potential miscalibration of scattering signals remains. Therefore we retain the Liu et al. (2014) separation line between traffic and wood burning BC as plausible for identifying wood burning particles. Moreover, variability in mixing state introduces uncertainties into climate models that assume immediately internal mixing of primary BC and OM (Ting et al., 2018). Our results confirmed that only a fraction of primary BC and OM is internally mixed when emitted, and that this mixing varies by user operations, which may bias model estimation for BC radiative forcing. The absence of thickly coated BC comparing to previous ambient studies (Liu et al., 2014; Liu et al., 2019) may reflect the effectiveness of smoke control policies including both fuel and appliance restrictions.

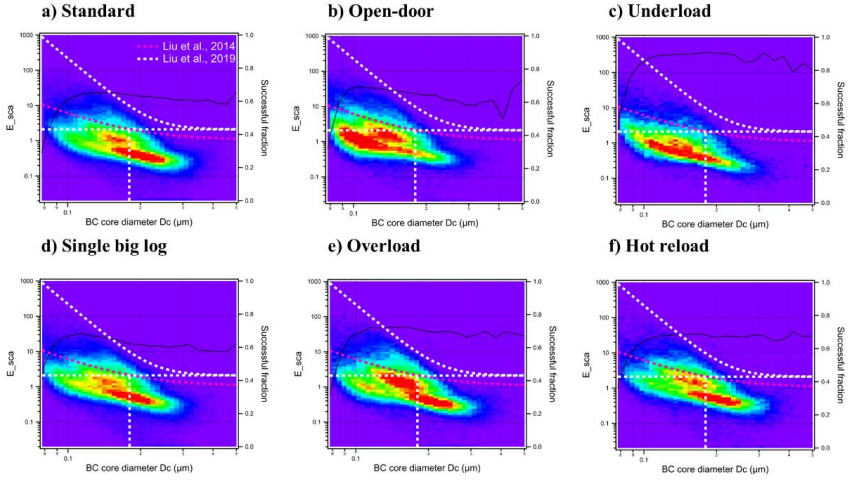

Figure 5 Scattering enhancement (E_{sca}) as function of BC core diameter (D_c) for different stove operations. Each panel shows a 2-D histogram of detected rBC containing particles (Liu et al., 2014; Liu et al., 2019; Joshi et al., 2021; Cheng et al., 2025), coloured by particle number density; red denotes > 70% of the burn maxima. Each panel is retrieved from the whole day experiment including several flaming phases of burn cycles, excluding kindling and chamber. Dashed pink curves are the reference lines to mark traffic and solid fuel burning BC (Liu et al., 2014). Dashed white curves classify BC particles into four groups based on coating thickness and core size (Liu et al., 2019). Black solid lines show the number fraction of BC particles with successful LEO fits.

3.3.2 Particle size distributions

Accumulation mode particles from wood burning mainly emitted during flaming phases (Fig. 6). Rich flaming primarily emitted particles with a unimodal size distribution, exhibiting a single peak at D_m = 190 nm (Fig. 6 b). In contrast, non-rich flaming produced bimodal size distributions, with a nucleation mode peaking at D_m = 20

https://doi.org/10.5194/ar-2026-24
Preprint. Discussion started: 30 June 2026

nm and an accumulation mode peaking at D_m = 190 nm (Fig. 6 c). Deviations from standard operation like opening stove door or underload the stove shifted the flaming phase size distribution toward smaller diameters. Panels b and c in Fig. 5 show a population of small, un-coated BC particles distributed around 0.1 µm, hereafter termed BC-containing ultrafine particles (BC-UFPs), under flaming phases of open-door and underload protocols. Consistent with BC-UFPs observations, distinct D_m peaks at 20 nm were observed for open-door protocol in both rich and non-rich flaming phases (Fig. 6 b, c; green curves). The open-door burn protocol effectively converts the stove into an unsealed system, shortening the residence time of combustion gases and nascent particles inside the firebox and then suppressing their condensation and coagulation, which is consistent with a previous study on monitoring wood burning emissions, where open burning produced smaller BC cores (Ting et al., 2018). However, UFPs were also observed under sealed protocols like underload (Fig. 5 c and Fig. 6 c) which can be due to low Brownian coagulations (Seinfeld and Pandis, 2016) resulting from low Brownian motion because low BC concentrations decrease collision frequencies (Pratsinis, 1988). The coagulation rate of particles is approximately proportional to the square of their concentrations; here, averaged mass concentrations for underload and open-door protocols were 4.38 µg m^{-3} and 12.9 µg m^{-3}, respectively, indicating that underload burn was 10 times and open-door burn 4 times lower than the standard burn protocol BC mass concentrations. As a result, a fraction of these UFPs can potentially be released into the flue before being oxidised or coagulated in the flame. Additionally, UFPs were also observed in overload burns (Fig. 5 e and Fig. 6 b, c). Overload burn leads to more non-homogenous flaming, where the stack is high enough to release emitted UFPs before being coagulated in the flame. Overall, maloperations such as underload and open-door burns produce less BC levels than the standard burn protocol but promoted BC-UFP emissions, whereas overload burn increased both BC and UFPs emissions, underscoring the importance of standard stove operation to mitigate UFP emissions. Hot reload and overload protocols produced a higher number of large particles (D_m > 100 nm) compared to the standard burn protocol. One possible explanation for the larger particle sizes is the increased availability of OM that becomes internally mixed with BC during rich flaming (Fig. 8 a, c, e).

https://doi.org/10.5194/ar-2026-24
Preprint. Discussion started: 30 June 2026

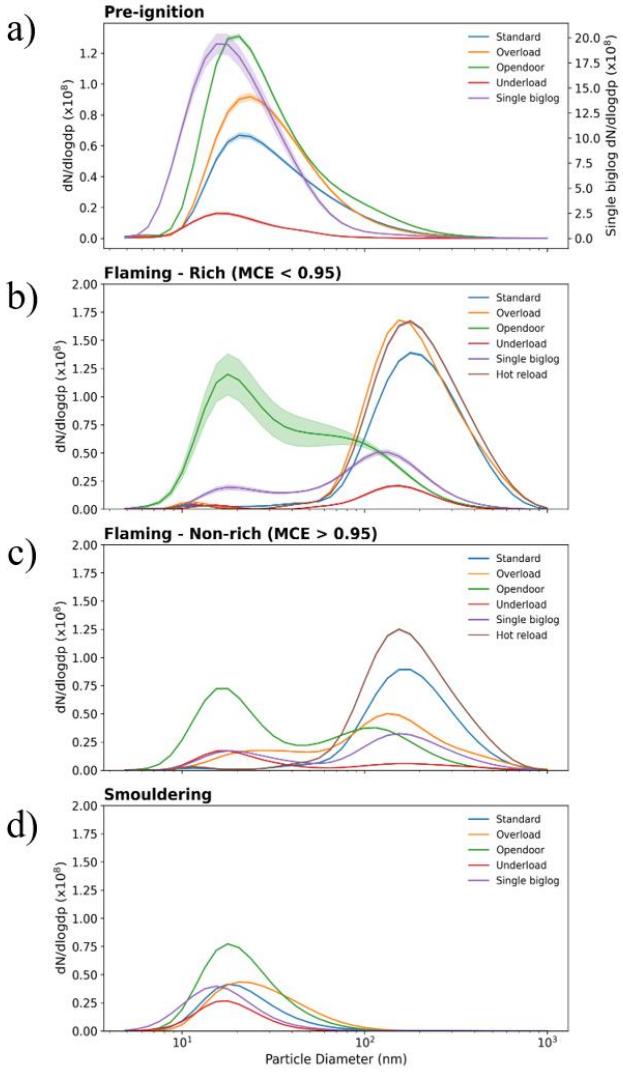

Figure 6 Particle size distribution (particle diameter D_m on x-axis) for pre-ignition (a), flaming (b, c) and smouldering (d) phases. The particle size distribution for each burn protocol is shown in different colours, each coloured line is the cumulative-averaged data of a whole day experiment including several burn cycles of the same phase. Shaded area are the standard errors. The size distribution of the pre-ignition phase of single big log protocol is multiplied by 0.1 to make it comparable with others.

Pre-ignition and smouldering size distributions (Fig. 6 a, d) are dominated (in number) by UFPs. A large UFP peak was observed during the pre-ignition phase of single big log protocols (Fig. 6 a, purple curve). This indicates that cutting the log to maximise contact area with embers enhances pre-ignition emissions. The underload protocol produced relatively low particle numbers among all protocols. While overload and open-door burn protocols produced a higher number of pre-ignition particles than the standard protocol. Consequently, fuel mass, firebox sealing and log-to-ember contact area can substantially modify UFP emissions by altering both the magnitude of UFP number concentrations and timing of their release during the burn cycle.

https://doi.org/10.5194/ar-2026-24
Preprint. Discussion started: 30 June 2026

These effects should be considered in emission inventories and exposure assessments, because short, intense bursts of UFP during pre-ignition and smouldering may contribute disproportionately to particle number exposure.

Particle size distributions measured in smouldering phases showed a similar pattern to the pre-ignition phases, with lower particle number concentrations limiting particle growth (lower variability and number in size distributions). Larger particles during smouldering were observed under overload protocol because of the high particle concentration enhancing coagulation and leading to the formation of larger particles. Conversely, the single big log protocol produced smaller particles during smouldering. This may reflect both the prior release of volatiles during pre-ignition and the higher surface area to volume ratio of the big log, which likely slowed the release of volatiles and reduced the availability of condensable material during smouldering.

Consequently, during the standard, hot-reload, and overload protocols, particle size distributions were dominated by an accumulation-mode peak near 100 nm. In contrast, the open-door, under-stack, and single-log protocols were characterized by enhanced UFP emissions, with peaks at $D_m \approx 10$ nm. Although the SP2 has limited ability to detect particles with a $D_m < 70$ nm ($D_m \approx 32$ nm) due to signal-to-noise issues, measurable incandescence signals suggests that wood stove combustion can emit BC containing UFPs during the flaming phases of the underload and open-door burns. Moreover, 30 - 100 nm UFPs can remain airborne for days which enhance the related health risks (Schraufnagel, 2020), and impact on climate by influencing cloud formation and precipitation (Junkermann and Hacker, 2018; Kwon et al., 2020). UFP emissions also dominated pre-ignition and smouldering phases across all protocols, yet there is no significant evidence that these particles contain BC (Junkermann and Hacker, 2018; Kwon et al., 2020).

3.3.3 BC particles coating

OM emitted during combustion can either condense onto rBC cores (internal mixing) or remain externally mixed and emitted separately. We quantified the extent of internal mixing using the bulk coating thickness (see Sect. 2.2.1). During a typical flaming phase, coating bulk decreased linearly with increasing MCE (Fig. 7; $R^2 = 0.90$), indicating that BC cores will gain progressively thicker OM coatings as combustion becomes less efficient. The tight correlation between coating thickness and MCE therefore underscores the sensitivity of BC mixing state to instantaneous combustion efficiency. Under low MCE, a large proportion of OM, especially PAHs, may prevent the BC particles from forming a core-shell morphology. The resulting heterogenous coating increases the scattering cross section at 1064 nm, which may lead to an overestimation of D_p.

https://doi.org/10.5194/ar-2026-24
Preprint. Discussion started: 30 June 2026

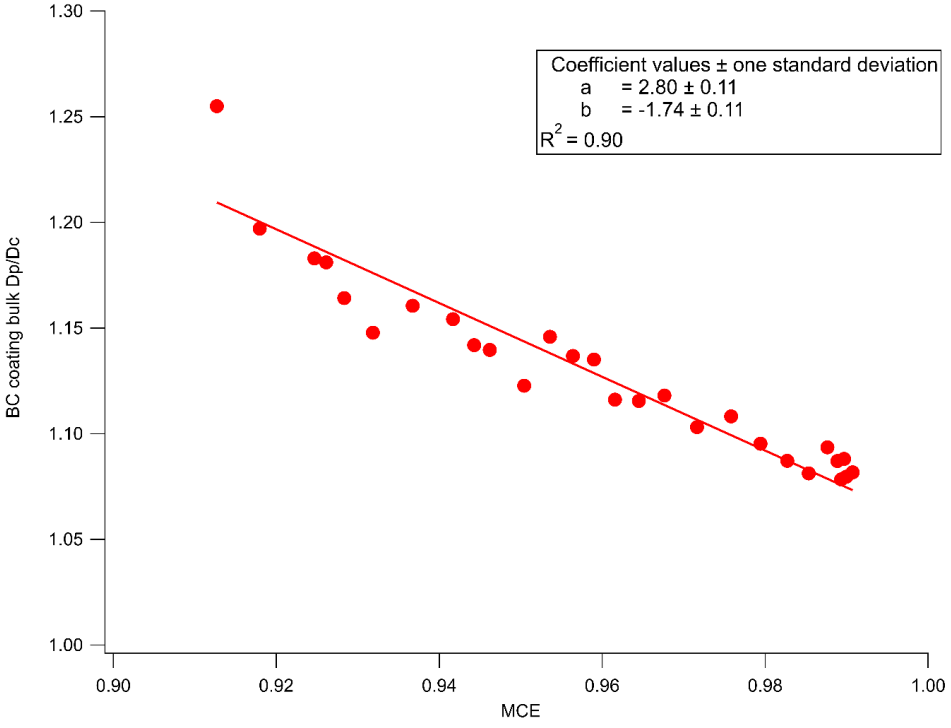

Figure 7 Orthogonal distance regression fit and Pearson correlation coefficient (R^2) between BC coating bulk (D_p/D_c) and MCE during a flaming phase under standard protocol. The fitted slope was -1.74 ± 0.11 and intercept was 2.80 ± 0.11.

E_{sca}- D_c distribution for non-rich (MCE > 0.95) and rich (MCE < 0.95) combustion are shown in Fig. 8 a – f, with the corresponding E_{sca} histograms in Fig. 8 g – i. BC concentrations during pre-ignition and smouldering phases are negligible comparing to flaming phase, so we only reported flaming phases here. Wood combustion is a complex process that pyrolysis, flaming and smouldering processes can simultaneously occur on different surfaces of a log, thus the observed mixing states and size distribution represent a combination of these processes. To maximize contrast between rich and non-rich flaming, we compared overload (predominantly rich burns) and underload (predominantly non-rich burns) protocols (Fig. 8 a, b). Hot-reload exhibited a mixture of the non-rich and rich conditions (989 s for rich and 2873 s for non-rich flaming as shown in Table 2). Rich combustion exhibited a bimodal mixing state distribution, with close to equal fractions of non-coated and coated BC particles (Fig. 8 a, c, e). While non-rich burns show a single mode mainly containing very thinly coated BC particle without clear boundary (Fig. 8 b, d, f). To better address the two groups, BC particles were classified according to the discontinuous distribution following Liu et al. (2019), the criteria is shown as black dashed line in Fig. 8. Particles lying above these criteria were classified as thickly coated BC, which were mainly observed in rich burns (Fig. 8). The averaged concentration of thickly coated BC during rich flaming was higher than non-rich flaming across all protocols (Table 2). This indicates that additional OM emitted from rich burns condenses onto or coagulated with BC cores. Importantly, the E_{sca} mode remains consistent across protocols. This E_{sca} mode further corroborates the negative relationship between MCE and coating thickness shown in Fig. 7. Interestingly, large uncoated BC (D_c > 180 nm, E_{sca} < 2.1) was observed during rich flaming, which has not

https://doi.org/10.5194/ar-2026-24
Preprint. Discussion started: 30 June 2026

been observed in significant amounts in the UK wood burning dominant urban areas previously (Liu et al., 2014).

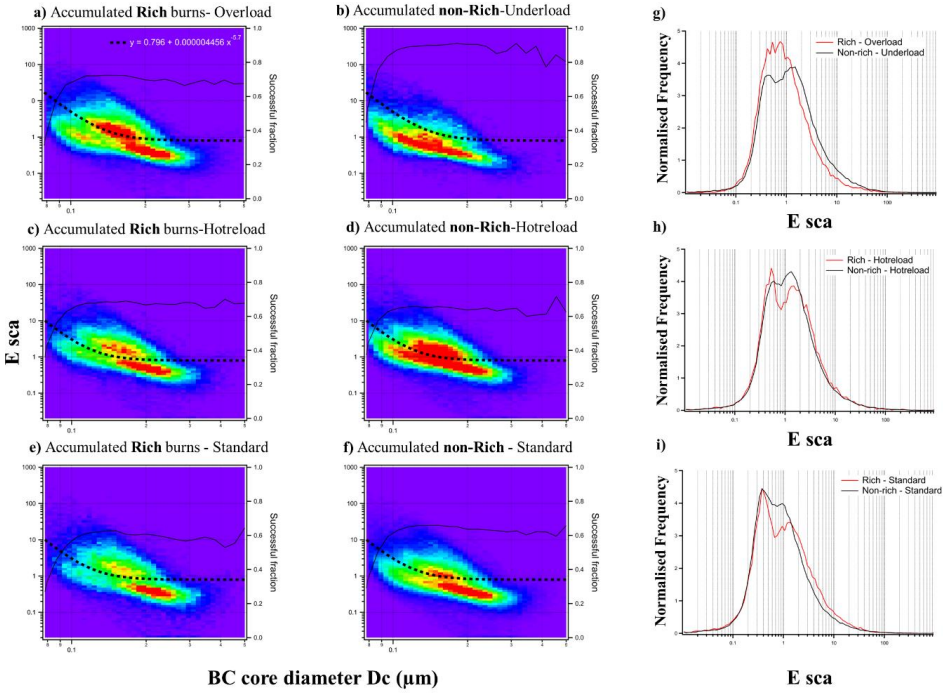

Figure 8 BC mixing state of rich and non-rich flaming E_{sca} (a-f) and histogram (g - i). The E_{sca} plots show data accumulate from rich (MCE < 0.95) and non-rich (MCE > 0.95) flaming across all repeats conducted on a single experiment day. The particles are classified by a criteria shown as black dashed line at $y=0.796 + 0.000004456 * x^{-5.7}$ to identify thickly coated BC and thinly coated BC.

In the open-door protocol, non-rich combustion produced additional thinly coated (E_{sca} from 1 to 2) BC particles with D_c < 100 nm (Fig. 9 a, c), a feature absents from other non-rich flaming phases (Fig. 8 b, d, f). The number concentration ratio rBC < 100 nm/ rBC > 100 nm was 0.69, more than 10 times higher than in the standard protocol (0.061). Particles from non-rich burns accounted for > 99 % of the total particles in the open-door protocol, these BC containing UFPs were associated with non-rich burns. The average flow temperature during open-door (220 ± 24.9 ºC) was slightly lower than standard protocol (230 ± 14.6 ºC). We propose that the continuous influx of cool lab air into the fire box disrupts the flame structure, producing local low temperatures. Simultaneously, low rBC concentration and cooling supressed particle growth and Brownian coagulation, preventing nucleation particles from forming accumulation mode particles (Seinfeld and Pandis, 2016). The open door will also cause inhomogeneities in the firebox in terms of temperature and oxygen availability, meaning that the combustion conditions are more complex.

https://doi.org/10.5194/ar-2026-24
Preprint. Discussion started: 30 June 2026

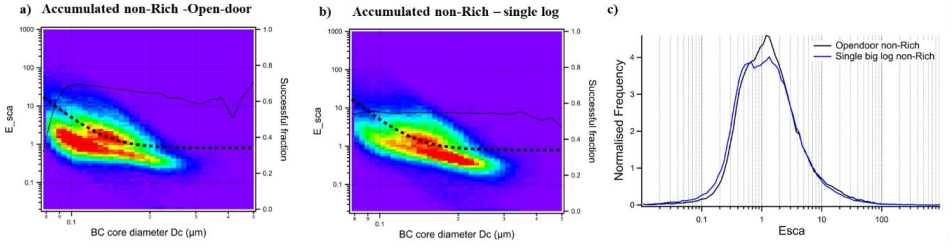

Figure 9 BC mixing state metric E_{sca} plots during non-rich flaming under open door protocol (a), single big log protocol (b) with corresponding histogram (c).

3.3.4 BC core size

Stove maloperation can shift the rBC core size distribution toward smaller diameters relative to the standard protocol (Fig. 10). However, correlations between MCE and BC core size are not obvious (Fig. S3). This contrasts with Ting et al. (2018), who reported an increase in BC core size with MCE for a sealed pre-Ecodesign heating stove, although no clear correlation was observed for open burning. This difference from the previous study may reflect the complexity of log combustion, where MCE represents a bulk combustion metric but rBC core size is controlled by particel growth, residence time and local flame conditions. The size distributions in Fig. 10 are not in ideal lognormal curves, with an additional particle population observed between 70 nm and 100 nm, particularly during overload rich flaming, open-door and underload non-rich flaming. This sub-100 nm mode suggests that BC-UFPs are present across the burn protocols, but their relative contribution is enhanced under protocols that reduced particle residence time. Rich combustion produced slightly larger BC cores than non-rich combustion (Fig. 10), implying rich combustion promotes coagulation among nascent rBC particles because of the additional internally mixed OM. In addition, D_c peaks at 0.19 μm during standard rich flaming and at 0.17 μm during standard non-rich flaming, whereas the corresponding modes during hot reload are similar, at 0.17 μm and 0.16 μm respectively. The weak separation between rich and non-rich flaming during hot-reload suggests that rich and non-rich combustion may occur simultaneously in different layers or on different surfaces of the logs, masking any simple relationship between MCE and rBC core size.

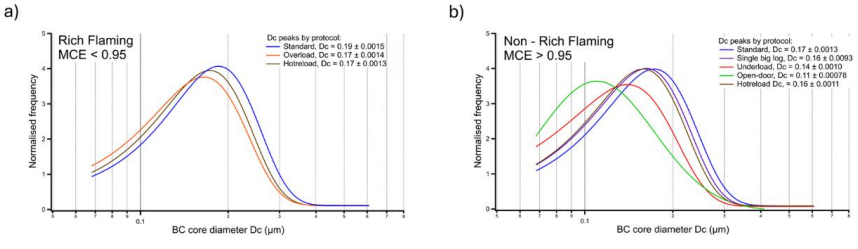

Figure 10 BC core size distribution of selected rich and non-rich burns with threshold MCE=0.95. The binned distribution is fitted as log normal from 70 nm to 600 nm which is the detection limit for SP2, where incandescence signal under 70 nm is highly affected by noise while larger than 600 nm is saturated.

https://doi.org/10.5194/ar-2026-24
Preprint. Discussion started: 30 June 2026

3.4 OM and BC external and internal mixing states among protocols

Figure 11 shows that the BC mixing state spans nearly the full range of mixing fraction, from fully internal (≈ 1.0) to highly external (≈ 0.1), across all protocols. This is consistent with the mechanism that high OM emissions lead to more external mixing (Ting et al., 2018). For protocols dominated by non-rich flaming, F_{in} decreased from fully internal to highly external with the OM mass fraction (OM/(OM+BC)). When OM fraction > 0.6, some rich combustion dominant protocols especially hot reload showed strong agreement between OM fraction and F_{in}. By contrast, non-rich flaming dominant protocols like single log and open-door showed a broad range F_{in} from 0.1 to 1.0. Which indicates MCE influences the mixing state, therefore we further compared F_{in} with MCE as shown in Fig. 12.

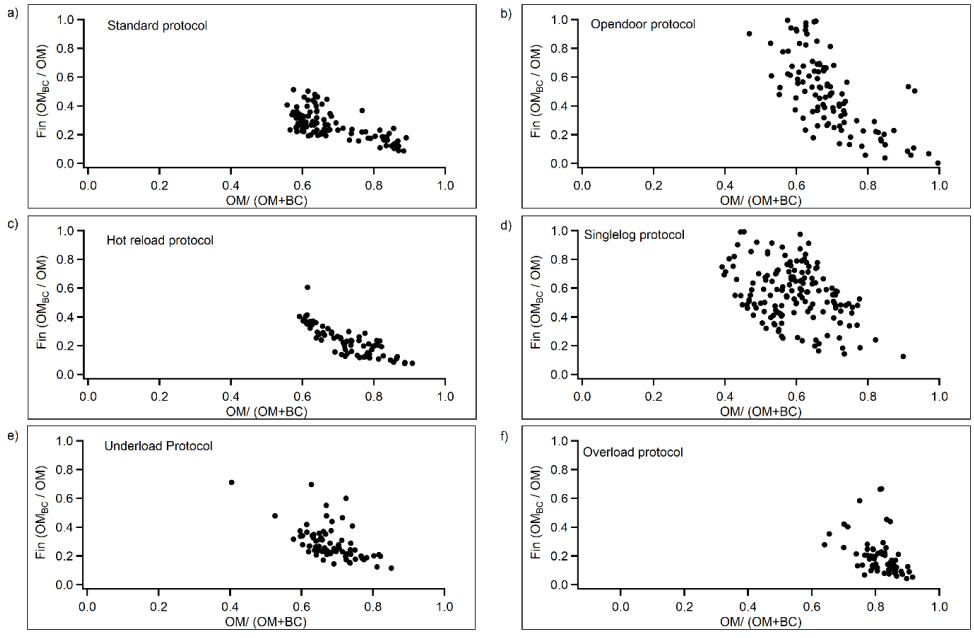

Figure 11 Internally mixed OM ratio F_{in} (OM_{BC}/OM) as a function of OM mass fraction (OM/(OM+BC)) during flaming phase of all protocols.

The average F_{in} for rich flaming (MCE < 0.95) was higher than non-rich flaming (MCE > 0.95) under the standard, hot reload and overload protocols (Table 2), consistent with pre-Ecodesign stove results (Ting et al., 2018). For most protocols, F_{in} increased with MCE from almost all external mix to highly internal mixing, except overload and underload (Fig. 12). When MCE approaches unity, the F_{in} distribution is broad (0.1 to 1.0), which may indicate even under efficient (near unity MCE) combustions, the BC mixing states were heterogeneous. BC can be both non- coated and coated, further reflecting spatial heterogeneity among pyrolysis, flaming and smouldering occur simultaneously on different surfaces/layers of the wood log.

However, in the underload protocol, F_{in} decreases from 0.6 to 0.2 when MCE are approaching 1. This may indicate during highly efficient combustions, abundant oxygen and limited condensable materials can supress the internally mixed of BC and OM, because some VOCs were oxidised before they can condense onto BC. Overload protocol shows no significant correlation (Spearman rank close to 0) between F_{in} and MCE. The F_{in}

https://doi.org/10.5194/ar-2026-24
Preprint. Discussion started: 30 June 2026

ranged from < 0.1 to 0.6 as MCE varied, consistent with the simultaneous emission of bare and coated BC described in Sect. 3.3.1.

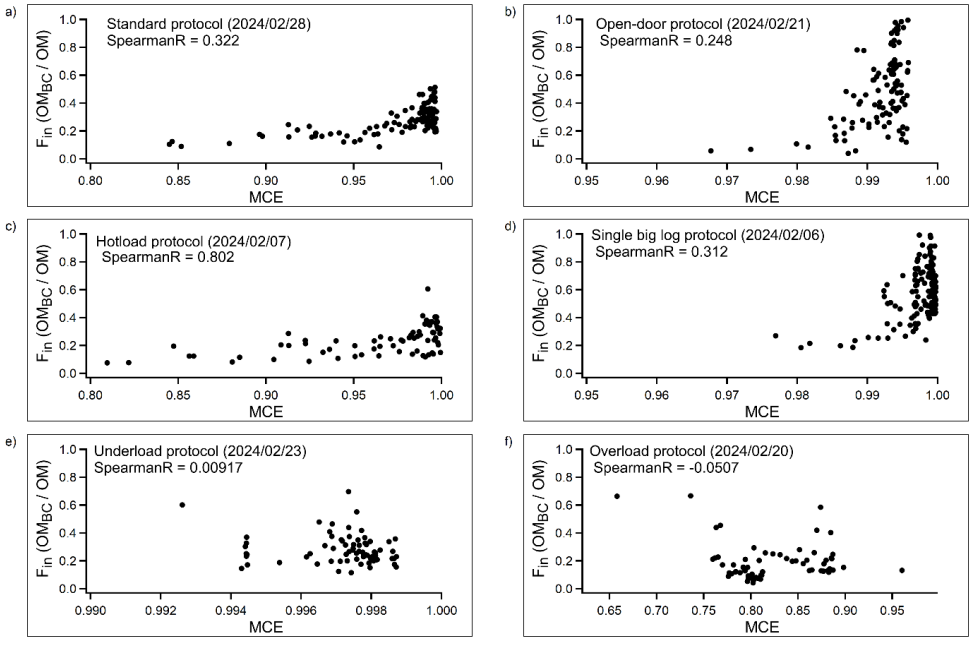

Figure 12 Internally mixed OM ratio F_{in} (OM_{BC}/OM) as a function of MCE during all protocols in flaming phases.

3.5 Top – down ignition test

The top-down ignition test was conducted as one burn cycle. As expected, the DMS500 size distributions showed no clearly defined pre-ignition phase (Fig. S16 b), despite the burn being initiated from a cold stove. Instead, particle number was dominated by large particles (D_m peaks at 20nm) from the start of ignition, rather than by the smaller particles (D_m peaks at 190nm) observed during pre-ignition phase of the standard protocol. During flaming phase, the organic aerosol concentration (at level of 45-50 µg m^{-3}) remained lower than the BC concentrations (at level of 100 µg m^{-3}) for the first seven minutes (Fig. S18 d), which contrasts with the standard log reload burn cycles. After seven minutes, probably the kindling wood pieces were consumed, the rBC and OM concentration remain at the same level at 50 µg m^{-3}.The AMS mass spectra (Fig. S17) also showed limited contributions from small organic fragments compared with the standard protocol, suggesting that a fraction of VOCs released during ignition may have passed through and been oxidised within the flame above the logs. In this single run, no rich flaming phase was observed, and the MCE remained above 0.95 throughout the burn (Fig. S18 a). This provides preliminary evidence that top-down ignition may suppress the development of rich flaming. Together with the hot reload results, this observation reinforces the interpretation that a substantial fraction of emissions arises from pyrolysis products released from the logs that do not pass directly through an active flame zone before entering the flue. However, this interpretation is based on a single top-down ignition experiment, which indicates it needs more repeatable experiments to prove. Moreover, top-down ignition is only

https://doi.org/10.5194/ar-2026-24
Preprint. Discussion started: 30 June 2026

applicable to start up the stove and cannot be directly applied during reloading. Therefore, rich flaming may still occur when fresh logs are loaded to an existing ember bed.

3.6 Implications among Protocols

Table 2 Averaged rBC number and mass concentrations, coating bulk, MCE, F_{in} and core size of flaming phase for each protocol. The uncertainties are standard deviation.

Protocols	Standard		Hot-reload		Open-door	Overload		Single big log non-rich
Flaming conditions	Rich flaming	Non-Rich flaming	Rich flaming	Non-Rich flaming	Non-Rich flaming	Rich flaming	Non-Rich flaming	Non-Rich flaming
Averaged rBC mass concentration ($\mu g\ m^{-3}$)	67.20 ± 23.30	46.00 ± 21.70	50.9 ± 16.2	33.80 ± 16.30	14.20 ± 15.10	59.10 ± 23.80	7.80 ± 7.85	21.60 ± 23.90
Averaged rBC number concentration (cm^{-3})	9419 ± 1615	8246 ± 2557	8784 ± 1933	7508 ± 2845	5598 ± 3425	11100 ± 2335	2356 ± 1504	4779 ± 3989
Averaged thickly coated rBC mass concentration ($\mu g\ m^{-3}$)	8.65 ± 3.63	5.50 ± 3.24	8.96 ± 4.12	4.81 ± 3.67	3.03 ± 2.33	7.28 ± 3.91	1.76 ± 2.27	3.75 ± 3.48
Averaged Coating Bulk	1.14 ± 0.14	1.11 ± 0.09	1.14 ± 0.07	1.12 ± 0.07	1.180 ± 0.089	1.14 ± 0.07	1.18 ± 0.11	1.18 ± 0.12
Duration (s)	697	3646	989	2873	3924	2128	395	5430
Averaged MCE	0.910 ± 0.038	0.99 ± 0.011	0.840 ± 0.076	0.990 ± 0.012	0.990 ± 0.011	0.830 ± 0.062	0.99 ± 0.01	1.000 ± 0.008
Averaged F_{in}	0.160 ± 0.042	0.300 ± 0.089	0.150 ± 0.062	0.28 ± 0.16	0.49 ± 0.25	0.19 ± 0.13	-	0.58 ± 0.19
Averaged Core cmd (μm)	0.160 ± 0.017	0.140 ± 0.022	0.150 ± 0.013	0.130 ± 0.033	0.010 ± 0.017	0.140 ± 0.014	0.100 ± 0.019	0.120 ± 0.020
Averaged Core mmd (μm)	0.240 ± 0.024	0.210 ± 0.037	0.230 ± 0.026	0.190 ± 0.054	0.160 ± 0.030	0.220 ± 0.025	0.170 ± 0.037	0.180 ± 0.038

https://doi.org/10.5194/ar-2026-24
Preprint. Discussion started: 30 June 2026

Underload non-rich	Non-Rich flaming	4.43 ± 5.29	1288 ± 1338	0.73 ± 1.14	1.13 ± 0.15	4144	0.99 ± 0.01	0.28 ± 0.11	0.120 ± 0.048	0.140 ± 0.057

Previous sections showed that aerosol size, chemical compositions and BC coating thickness varied across combustion phases, implying that the duration of each phase may strongly influence stove emissions. To test this, we paired phase durations across protocols and compared them using Student's T-test (unequal variances). The results indicate that pre-ignition and rich flaming duration differences are not incidental but protocol dependent (Fig. 13).

For rich flaming, 8 of 15 pairwise protocol contrasts were significant at $t > 2$, where 7 pairs of them were showing strong significance at $t > 3$. Overload protocol was significantly different from all other protocols (5 out of 5 pairs with $t > 3$). Hot reload protocol also tended to prolong the rich flaming, with significant contrast against underload ($t = 3.7$) and single big log ($t = 3.6$). Pre-ignition differences were also significant, with 8 of 15 pairwise protocol contrasts were significant at $t > 2$, and 3 of them were showing at $t > 3$. Hot reload and underload substantially suppressed pre-ignition phase, where hot reload suppression was due to manual operation. These results indicate that the choice of stove operating protocol produces reproducible shifts in pre-ignition and rich flaming duration.

Table 3 Pre-Ignition and Rich flaming duration (seconds) of all load cycles. With averaged duration, standard deviation and pair T test p value.

Protocols	Load cycle	Pre-ignition (s)	Rich Flaming (s)	Mean (pre)	Stedv (pre)	Mean (Rich)	Stedv (Rich)
	1	88	56.5				
Standard	3	75	0	55.3	37.4	122	134
	4	3	308.5				
	1	0	185				
Hot reload	2	0	431	0	0	308	100
	3	0	308				
	1	73	170.5				
Open-door	2	69	0	107	50.9	64	75.8
	3	179	21.5				
	1	13	1725				
Overload	2	3	1909	27	27.2	1810	76.6
	3	65	1785				
	1	85	35.5				
Single big log	2	76	0	65	47.1	37.2	31
	3	110	76				
	1	165	0				
Underload	2	143	78	138	24.3	26	36.8
	3	106	0				

https://doi.org/10.5194/ar-2026-24
Preprint. Discussion started: 30 June 2026

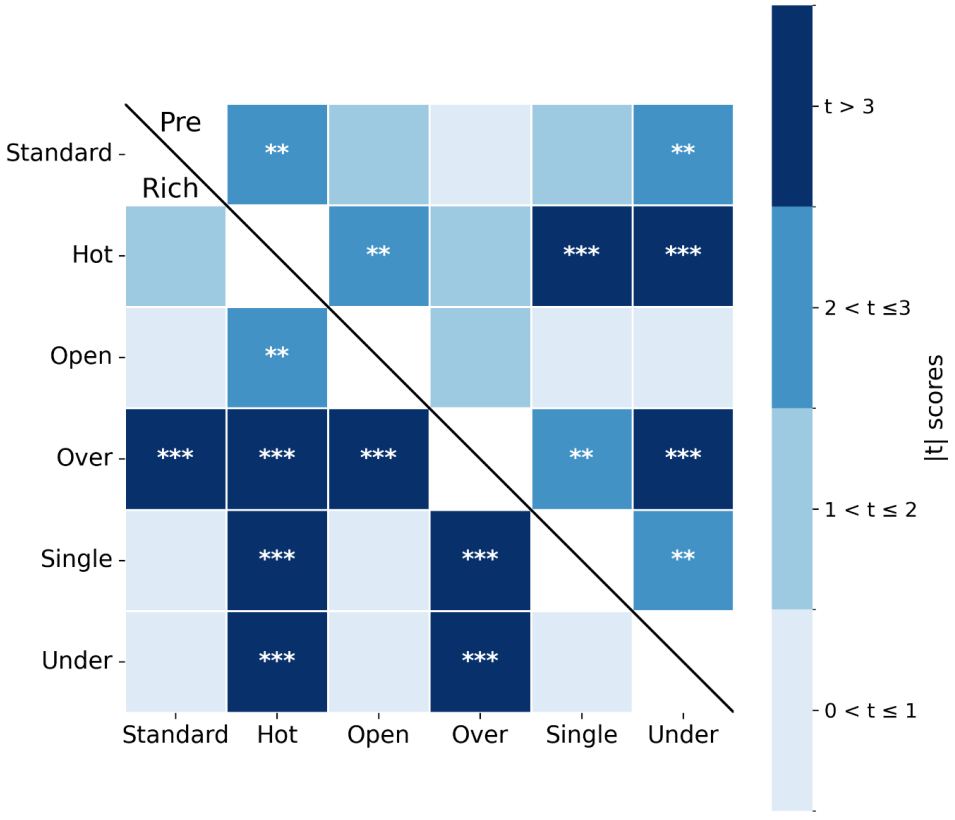

Figure 13 Heatmap of Student's T-test t-scores for pre-ignition phase (top right) and rich flaming phase (bottom left) phase durations (s); each 2 protocol durations were paired. To better visualize the significance, t-score > 3 pairs are marked as *, while 2 < t-score < 3 are marked as **.**

We attribute the significant durational differences to wood-log geometry, specifically the surface-to-volume ratio and the ember contact area (Sect. 3.3.2). A large surface-to-volume and ember contacts area, as in the single big log and underload protocols, extended pre-ignition but shorten rich flaming phases (Table 3). In practical stove operation, chopping fuel into smaller pieces is therefore likely to prolong the rich flaming phase which produces BC with thicker coatings (Table 2) and elevates PAHs emissions (Sect. 3.2). Compared with the standard protocol, hot-reload facilitates ignition because logs were loaded during the flaming phase, however, the associated extension of the rich flaming phase (Fig. 13) significantly increases the potential of high PAHs and thickly coated BC emissions. The overload protocol also increased the flaming duration for each load (Table 2 and 3) which reduced the frequency of reloads in real world stove operation, however, its extended rich flaming phase (Fig. 13) would increase emissions. Open-door protocol reduced BC concentrations, BC coating thickness and PAH emissions, however, it increased the health risk by producing more UFPs. In contrast, underload and single big log protocols were not easy to ignite owing to their longer pre-ignition phases, however, they

https://doi.org/10.5194/ar-2026-24
Preprint. Discussion started: 30 June 2026

decreased rich flaming duration and thereby reduced thickly coated BC and PAHs emissions, making them advantageous options for minimising aerosol emissions.

4. Conclusions

This study provides key emission characteristics of carbonaceous aerosol from a modern Ecodesign stove when burning dry Ashwood, including BC concentrations, particle size distributions, mixing states and chemical compositions. Overall, modern Ecodesign stoves burn wood with higher efficiency (high MCE) when operated properly (based on a standard burn protocol). However these stoves can potentially exhibit unfavourable emission behaviours (e.g., increased emissions of thickly coated BC and PAHs) based on usage that deviates from the standard protocol, as mentioned in previous studies (Allan et al., 2025).

Therefore, this study also measured emission variabilities under deviations from standard operation. The emissions were highly variable based on the combustion phases observed, where rich combustion was a key regime driving changes in BC core size, mixing state and chemical composition. Larger BC cores were observed during rich flaming (Averaged MMD 0.24 µm, standard protocol) compared with non-rich (Averaged MMD 0.21 µm, standard protocol), with core diameter varying among protocols based on the MCE. A robust bimodal BC mixing state, including thinly and thickly coated BC, was observed and quantified for the burn protocols. Thickly coated BC formed mainly during rich flaming due to higher OM availability, consistent with increased external mixing (low F_{in}). Chemical composition of the particles emitted during burning depended highly on combustion phases where pre-ignition and smouldering produced more saturated hydrocarbons such as alkanes whereas flaming phase, especially rich flaming, produced more PAHs.

Burning dry Ashwood in an Ecodesign stove using varying different burn protocols influences particle emissions through two principal pathways. First, overload and hot reload potentially increase the rich flaming duration (by a factor of nine) comparing to standard protocol, thereby increasing emissions of PAHs and thickly coated BC. This shift in particle chemical composition may increase potential health risks due to the toxicity of PAHs. This may also enhance the absorption of the BC containing particles through lensing effects. Second, underload and open-door protocols shorten particle residence time in the stove and therefore increase UFP emissions. If not efficiently filtered, these UFPs pose additional human health risks because their small size can prolong their airborne residence time, enable deposition deep in the lungs and reduce the respiratory capacity. Overall, the standard and single “big log” burn protocols led to relatively low PAHs, UFPs and thickly coated BC emissions comparing with the overload, hot-reload, underload and open-door protocols. Thus, these two low emission burn protocols are recommended when burning dry Ashwood in Ecodesign stoves to reduce wood burning emissions.

MCE is widely reported as a single variable to monitor emissions in wood combustion studies. However, reliance on MCE alone may be misleading because pre-ignition, rich flaming, and smouldering phases can all reduce MCE via distinct physiochemical mechanisms. This work presents significant differences in emission characteristics such as particle size and chemical composition among these phases. We therefore recommend reporting phase-resolved MCE (e.g., flaming MCE) for MCE based emission monitoring. However, MCE will not be sufficient to parameterise the abundant pre-ignition emissions, which intrinsically take place outside of the combustion process.

https://doi.org/10.5194/ar-2026-24
Preprint. Discussion started: 30 June 2026

The insight gathered here on the modes of emission will also have implications for the operating methods of domestic stoves, as it demonstrates that much of the previously-documented adverse emissions of modern stoves when burning dry wood occur when they are used outside of their operating conditions. In particular, when too much wood is used, or with too high a surface area, rich combustion occurs because the combustible vapours are produced too quickly for the air system. This in turn produces an abundance of CO and PAHs. This can be remedied through user behaviour, in particular not overloading the appliance and using larger pieces of wood.

Acknowledgements

We thank Esse for the technical support with the stove and useful conversations regarding user behaviours.

Financial support

The CLARISE project was funded by the UK Natural Environment Research Council (Ref: NE/X000923/1).

Data availability

The CLARISE data will be available at https://archive.ceda.ac.uk/.

Author contribution

ZC made BC measurements with SP2, analysed SP2, AMS, DMS500 data. ZC wrote the paper and produced all figures. JA designed the research. HC, GM, JFH, AL, AR helped design the experiments. ZC, DK, LK, JA performed everyday experiments. AL, DW, DB, MF, MS, JRH helped setup the instruments. MF helped instrument calibration and alignment. JA processed raw AMS data with QA/QC. All authors read and commented on the paper.

Competing interests

The authors declare no conflict of interest.

Disclosure

This work is based on Chapter 3 of ZC's PhD thesis. This work was included in the thesis for the purposes of the PhD examination and was subsequently deposited. The thesis is available at: https://research.manchester.ac.uk/en/studentTheses/quantifying-uk-urban-black-carbon-emissions-using-multiple-techni/. This work had not been submitted to any journal or other publication prior to this submission.

https://doi.org/10.5194/ar-2026-24
Preprint. Discussion started: 30 June 2026

References

Alfarra, M. R., Prevot, A. S. H., Szidat, S., Sandradewi, J., Weimer, S., Lanz, V. A., Schreiber, D., Mohr, M., and Baltensperger, U.: Identification of the Mass Spectral Signature of Organic Aerosols from Wood Burning Emissions, Environmental Science & Technology, 41, 5770-5777, 10.1021/es062289b, 2007.

Allan, J., Cottrill, S., Churchill, S., Jones, J., Lea-Langton, A., Price-Allison, A., Stewart, R., Tarnawski, K., Williams, A., and Yardley, R.: EMISSION FACTORS FOR DOMESTIC SOLID FUELS PROJECT -WORK PACKAGE 1 REPORT, 2024a.

Allan, J., Cottrill, S., Churchill, S., Ingledew, D., Jones, J., Lea-Langton, A., Leonard, A., Stewart, R., Tarnawski, K., Williams, A., and Willis, D.: EMISSION FACTORS FOR DOMESTIC SOLID FUELS Work Package 2 Report, 2024b.

Allan, J., Cottrill, S., Churchill, S., Ingledew, D., Jones, J., Lea-Langton, A., Leonard, A., Quinn, P., Stewart, R., Tarnawski, K., Williams, A., and Willis, D.: EMISSION FACTORS FOR DOMESTIC SOLID FUELS Work Package 3 Report, 2025.

Bond, T. C. and Bergstrom, R. W.: Light Absorption by Carbonaceous Particles: An Investigative Review, Aerosol Science and Technology, 40, 27-67, 10.1080/02786820500421521, 2006.

Bond, T. C., Habib, G., and Bergstrom, R. W.: Limitations in the enhancement of visible light absorption due to mixing state, Journal of Geophysical Research: Atmospheres, 111, https://doi.org/10.1029/2006JD007315, 2006.

Bond, T. C., Streets, D. G., Yarber, K. F., Nelson, S. M., Woo, J.-H., and Klimont, Z.: A technology-based global inventory of black and organic carbon emissions from combustion, Journal of Geophysical Research: Atmospheres, 109, https://doi.org/10.1029/2003JD003697, 2004.

Bond, T. C., Doherty, S. J., Fahey, D. W., Forster, P. M., Berntsen, T., Deangelo, B. J., Flanner, M. G., Ghan, S., Kärcher, B., Koch, D., Kinne, S., Kondo, Y., Quinn, P. K., Sarofim, M. C., Schultz, M. G., Schulz, M., Venkataraman, C., Zhang, H., Zhang, S., Bellouin, N., Guttikunda, S. K., Hopke, P. K., Jacobson, M. Z., Kaiser, J. W., Klimont, Z., Lohmann, U., Schwarz, J. P., Shindell, D., Storelvmo, T., Warren, S. G., and Zender, C. S.: Bounding the role of black carbon in the climate system: A scientific assessment, Journal of Geophysical Research Atmospheres, 118, 5380-5552, 10.1002/jgrd.50171, 2013.

Brandelet, B., Rose, C., Rogaume, C., and Rogaume, Y.: Impact of ignition technique on total emissions of a firewood stove, Biomass and Bioenergy, 108, 15-24, https://doi.org/10.1016/j.biombioe.2017.10.047, 2018.

Canagaratna, M. R., Jayne, J. T., Jimenez, J. L., Allan, J. D., Alfarra, M. R., Zhang, Q., Onasch, T. B., Drewnick, F., Coe, H., Middlebrook, A., Delia, A., Williams, L. R., Trimborn, A. M., Northway, M. J., DeCarlo, P. F., Kolb, C. E., Davidovits, P., and Worsnop, D. R.: Chemical and microphysical characterization of ambient aerosols with the aerodyne aerosol mass spectrometer, Mass Spectrometry Reviews, 26, 185-222, https://doi.org/10.1002/mas.20115, 2007.

Cappa, C. D., Onasch, T. B., Massoli, P., Worsnop, D. R., Bates, T. S., Cross, E. S., Davidovits, P., Hakala, J., Hayden, K. L., Jobson, B. T., Kolesar, K. R., Lack, D. A., Lerner, B. M., Li, S.-M., Mellon, D., Nuaaman, I., Olfert, J. S., Petäjä, T., Quinn, P. K., Song, C., Subramanian, R., Williams, E. J., and Zaveri, R. A.: Radiative Absorption Enhancements Due to the Mixing State of Atmospheric Black Carbon, Science, 337, 1078-1081, 10.1126/science.1223447, 2012.

Cheng, Z., Hu, D., Flynn, M., Nemitz, E., Langford, B., Drysdale, W., Helfter, C., Cliff, S., Liu, D., Joshi, R., Cash, J., Lee, J., Coe, H., and Allan, J.: Quantifying black carbon emissions from traffic and construction in

https://doi.org/10.5194/ar-2026-24
Preprint. Discussion started: 30 June 2026

central London using eddy covariance, Environmental Science: Atmospheres, 5, 785-800, 10.1039/D5EA00039D, 2025.

Chowdhury, S., Pillarisetti, A., Oberholzer, A., Jetter, J., Mitchell, J., Cappuccilli, E., Aamaas, B., Aunan, K., Pozzer, A., and Alexander, D.: A global review of the state of the evidence of household air pollution's contribution to ambient fine particulate matter and their related health impacts, Environment International, 173, 107835, https://doi.org/10.1016/j.envint.2023.107835, 2023.

Cincinelli, A., Guerranti, C., Martellini, T., and Scodellini, R.: Residential wood combustion and its impact on urban air quality in Europe, Current Opinion in Environmental Science & Health, 8, 10-14, https://doi.org/10.1016/j.coesh.2018.12.007, 2019.

Elliott, M., Ingledew, D., Richmond, B., Del Vento, S., Gorji, S., Howes, S., Karagianni, E., Kelsall, A., Pang, Y., Passant, N., Pearson, B., Richardson, J., Stewart, R., Thistlethwaite, G., Tsagatakis, I., Wakeling, D., Wiltshire, J., Wong, J., Hobson, M., Gibbs, M., Dore, C., Thornton, A., Anthony, S., Carswell, A., Gilhespy, S., Cardenas, L., Dragosits, U., and Tomlinson, S.: UK Informative Inventory Report (1990 to 2023), 2025.

Eriksson, A. C., Nordin, E. Z., Nyström, R., Pettersson, E., Swietlicki, E., Bergvall, C., Westerholm, R., Boman, C., and Pagels, J. H.: Particulate PAH Emissions from Residential Biomass Combustion: Time-Resolved Analysis with Aerosol Mass Spectrometry, Environmental Science & Technology, 48, 7143-7150, 10.1021/es500486j, 2014.

Font, A., Ciupek, K., Butterfield, D., and Fuller, G. W.: Long-term trends in particulate matter from wood burning in the United Kingdom: Dependence on weather and social factors, Environmental Pollution, 314, 120105, https://doi.org/10.1016/j.envpol.2022.120105, 2022.

Fuller, K. A., Malm, W. C., and Kreidenweis, S. M.: Effects of mixing on extinction by carbonaceous particles, Journal of Geophysical Research: Atmospheres, 104, 15941-15954, https://doi.org/10.1029/1998JD100069, 1999.

Gao, R. S., Schwarz, J. P., Kelly, K. K., Fahey, D. W., Watts, L. A., Thompson, T. L., Spackman, J. R., Slowik, J. G., Cross, E. S., Han, J. H., Davidovits, P., Onasch, T. B., and Worsnop, D. R.: A Novel Method for Estimating Light-Scattering Properties of Soot Aerosols Using a Modified Single-Particle Soot Photometer, Aerosol Science and Technology, 41, 125-135, 10.1080/02786820601118398, 2007.

Haslett, S. L., Thomas, J. C., Morgan, W. T., Hadden, R., Liu, D., Allan, J. D., Williams, P. I., Keita, S., Liousse, C., and Coe, H.: Highly controlled, reproducible measurements of aerosol emissions from combustion of a common African biofuel source, Atmos. Chem. Phys., 18, 385-403, 10.5194/acp-18-385-2018, 2018.

Highwood, E. J. and Kinnersley, R. P.: When smoke gets in our eyes: The multiple impacts of atmospheric black carbon on climate, air quality and health, Environment International, 32, 560-566, https://doi.org/10.1016/j.envint.2005.12.003, 2006.

Hu, D., Alfarra, M. R., Szpek, K., Langridge, J. M., Cotterell, M. I., Flynn, M. J., Shao, Y., Voliotis, A., Du, M., Liu, D., Johnson, B., McFiggans, G., Haywood, J. M., Coe, H., and Allan, J.: Refractive Index of Engine-Emitted Black Carbon and the Influence of Organic Coatings on Optical Properties, Journal of Geophysical Research: Atmospheres, 128, e2023JD039178, https://doi.org/10.1029/2023JD039178, 2023.

Hu, D., Alfarra, M. R., Szpek, K., Langridge, J. M., Cotterell, M. I., Belcher, C., Rule, I., Liu, Z., Yu, C., Shao, Y., Voliotis, A., Du, M., Smith, B., Smallwood, G., Lobo, P., Liu, D., Haywood, J. M., Coe, H., and Allan, J. D.: Physical and chemical properties of black carbon and organic matter from different combustion and

https://doi.org/10.5194/ar-2026-24
Preprint. Discussion started: 30 June 2026

photochemical sources using aerodynamic aerosol classification, Atmos. Chem. Phys., 21, 16161-16182, 10.5194/acp-21-16161-2021, 2021.

Jetter, J., Zhao, Y., Smith, K. R., Khan, B., Yelverton, T., DeCarlo, P., and Hays, M. D.: Pollutant Emissions and Energy Efficiency under Controlled Conditions for Household Biomass Cookstoves and Implications for Metrics Useful in Setting International Test Standards, Environmental Science & Technology, 46, 10827-10834, 10.1021/es301693f, 2012.

Joshi, R., Liu, D., Nemitz, E., Langford, B., Mullinger, N., Squires, F., Lee, J., Wu, Y., Pan, X., Fu, P., Kotthaus, S., Grimmond, S., Zhang, Q., Wu, R., Wild, O., Flynn, M., Coe, H., and Allan, J.: Direct measurements of black carbon fluxes in central Beijing using the eddy covariance method, Atmospheric Chemistry and Physics, 21, 147-162, 10.5194/acp-21-147-2021, 2021.

Junkermann, W. and Hacker, J. M.: Ultrafine Particles in the Lower Troposphere: Major Sources, Invisible Plumes, and Meteorological Transport Processes, Bulletin of the American Meteorological Society, 99, 2587-2602, https://doi.org/10.1175/BAMS-D-18-0075.1, 2018.

Kantar: Research to understand burning in UK homes and gardens - AQ1017, https://randd.defra.gov.uk/ProjectDetails?ProjectID=20159&FromSearch=Y&Publisher=1&SearchText=AQ1017&SortString=ProjectCode&SortOrder=Asc&Paging=10#Description, 2020.

Klimont, Z., Kupiainen, K., Heyes, C., Purohit, P., Cofala, J., Rafaj, P., Borken-Kleefeld, J., and Schöpp, W.: Global anthropogenic emissions of particulate matter including black carbon, Atmos. Chem. Phys., 17, 8681-8723, 10.5194/acp-17-8681-2017, 2017.

Klimont, Z., Cofala, J., Xing, J., Wei, W., Zhang, C., Wang, S., Kejun, J., Bhandari, P., Mathur, R., Purohit, P., Rafaj, P., Chambers, A., Amann, M., and Hao, J.: Projections of SO2, NOx and carbonaceous aerosols emissions in Asia, Tellus B: Chemical and Physical Meteorology, 61, 602-617, 10.1111/j.1600-0889.2009.00428.x, 2009.

Kwon, H.-S., Ryu, M. H., and Carlsten, C.: Ultrafine particles: unique physicochemical properties relevant to health and disease, Experimental & Molecular Medicine, 52, 318-328, 10.1038/s12276-020-0405-1, 2020.

Lea-Langton, A. R., Spracklen, D. V., Arnold, S. R., Conibear, L. A., Chan, J., Mitchell, E. J. S., Jones, J. M., and Williams, A.: PAH emissions from an African cookstove, Journal of the Energy Institute, 92, 587-593, https://doi.org/10.1016/j.joei.2018.03.014, 2019.

Lee, A. K. Y., Rivellini, L.-H., Chen, C.-L., Liu, J., Price, D. J., Betha, R., Russell, L. M., Zhang, X., and Cappa, C. D.: Influences of Primary Emission and Secondary Coating Formation on the Particle Diversity and Mixing State of Black Carbon Particles, Environmental Science & Technology, 53, 9429-9438, 10.1021/acs.est.9b03064, 2019.

Li, Y. J., Yeung, J. W. T., Leung, T. P. I., Lau, A. P. S., and Chan, C. K.: Characterization of Organic Particles from Incense Burning Using an Aerodyne High-Resolution Time-of-Flight Aerosol Mass Spectrometer, Aerosol Science and Technology, 46, 654-665, 10.1080/02786826.2011.653017, 2012.

Liu, D., He, C., Schwarz, J. P., and Wang, X.: Lifecycle of light-absorbing carbonaceous aerosols in the atmosphere, npj Climate and Atmospheric Science, 3, 40, 10.1038/s41612-020-00145-8, 2020.

Liu, D., Allan, J. D., Young, D. E., Coe, H., Beddows, D., Fleming, Z. L., Flynn, M. J., Gallagher, M. W., Harrison, R. M., Lee, J., Prevot, A. S. H., Taylor, J. W., Yin, J., Williams, P. I., and Zotter, P.: Size distribution, mixing state and source apportionment of black carbon aerosol in London during wintertime, Atmos. Chem. Phys., 14, 10061-10084, 10.5194/acp-14-10061-2014, 2014.

https://doi.org/10.5194/ar-2026-24
Preprint. Discussion started: 30 June 2026

Liu, D., Joshi, R., Wang, J., Yu, C., Allan, J. D., Coe, H., Flynn, M. J., Xie, C., Lee, J., Squires, F., Kotthaus, S., Grimmond, S., Ge, X., Sun, Y., and Fu, P.: Contrasting physical properties of black carbon in urban Beijing between winter and summer, Atmos. Chem. Phys., 19, 6749-6769, 10.5194/acp-19-6749-2019, 2019.

Liu, D., Whitehead, J., Alfarra, M. R., Reyes-Villegas, E., Spracklen, Dominick V., Reddington, Carly L., Kong, S., Williams, Paul I., Ting, Y.-C., Haslett, S., Taylor, Jonathan W., Flynn, Michael J., Morgan, William T., McFiggans, G., Coe, H., and Allan, James D.: Black-carbon absorption enhancement in the atmosphere determined by particle mixing state, Nature Geoscience, 10, 184-188, 10.1038/ngeo2901, 2017.

Mărmureanu, L., Marin, C. A., Vasilescu, J., Petit, J.-E., Amodeo, T., Truong, F., Antonescu, B., Minguillon, M. C., Green, D. C., Zainab, B., Ovadnevaite, J., Elste, T., Coz, E., Allan, J., Croteau, P. L., Jayne, J., Canagaratna, M. R., Williams, L., Gros, V., Prevot, A. S. H., Favez, O., and Freney, E.: Evaluation of aerosol chemical speciation monitor response to different mixtures of organic and inorganic aerosols, Aerosol Science and Technology, 59, 16-33, 10.1080/02786826.2024.2412999, 2025.

Martinsson, J., Eriksson, A. C., Nielsen, I. E., Malmborg, V. B., Ahlberg, E., Andersen, C., Lindgren, R., Nyström, R., Nordin, E. Z., Brune, W. H., Svenningsson, B., Swietlicki, E., Boman, C., and Pagels, J. H.: Impacts of Combustion Conditions and Photochemical Processing on the Light Absorption of Biomass Combustion Aerosol, Environmental Science & Technology, 49, 14663-14671, 10.1021/acs.est.5b03205, 2015.

McMeeking, G. R., Kreidenweis, S. M., Baker, S., Carrico, C. M., Chow, J. C., Collett Jr, J. L., Hao, W. M., Holden, A. S., Kirchstetter, T. W., Malm, W. C., Moosmüller, H., Sullivan, A. P., and Wold, C. E.: Emissions of trace gases and aerosols during the open combustion of biomass in the laboratory, Journal of Geophysical Research: Atmospheres, 114, https://doi.org/10.1029/2009JD011836, 2009.

Michelsen, H. A., Schulz, C., Smallwood, G. J., and Will, S.: Laser-induced incandescence: Particulate diagnostics for combustion, atmospheric, and industrial applications, Progress in Energy and Combustion Science, 51, 2-48, 2015.

Mirme, A., Noppel, M., Peil, I., Salm, J., Tamm, E., and Tammet, H.: Multi-channel electric aerosol spectrometer, In Intern. Comm. for Cloud Phys. 11th Intern. Conf. on Atmosphere Aerosols, Nuclei, January 01, 1984, 155-159,

Mitchell, J., Gu, Y., Cottey, R., Chalmers-Arnold, I., Zhang, H., Thornton, A., Hampshire , K. A., Richmond , B., Thistlethwaite , G., and Willis, D. R.: Air Pollutant Inventories for England, Scotland, Wales and Northern Ireland: 2005-2022, https://naei.energysecurity.gov.uk/reports/air-pollutant-inventories-england-scotland-wales-and-northern-ireland-2005-2022, 2024.

Moteki, N., Kondo, Y., and Nakamura, S.-i.: Method to measure refractive indices of small nonspherical particles: Application to black carbon particles, Journal of Aerosol Science, 41, 513-521, https://doi.org/10.1016/j.jaerosci.2010.02.013, 2010.

Nichols, J. L., Owens, E. O., Dutton, S. J., and Luben, T. J.: Systematic review of the effects of black carbon on cardiovascular disease among individuals with pre-existing disease, International Journal of Public Health, 58, 707-724, 10.1007/s00038-013-0492-z, 2013.

Noonan, C. W., Ward, T. J., Navidi, W., Sheppard, L., Bergauff, M., and Palmer, C.: Assessing the impact of a wood stove replacement program on air quality and children's health, Research report (Health Effects Institute), 3-37, 2011.

https://doi.org/10.5194/ar-2026-24
Preprint. Discussion started: 30 June 2026

Orasche, J., Schnelle-Kreis, J., Schön, C., Hartmann, H., Ruppert, H., Arteaga-Salas, J. M., and Zimmermann, R.: Comparison of Emissions from Wood Combustion. Part 2: Impact of Combustion Conditions on Emission Factors and Characteristics of Particle-Bound Organic Species and Polycyclic Aromatic Hydrocarbon (PAH)-Related Toxicological Potential, Energy & Fuels, 27, 1482-1491, 10.1021/ef301506h, 2013.

Pagels, J., Dutcher, D. D., Stolzenburg, M. R., McMurry, P. H., Gälli, M. E., and Gross, D. S.: Fine-particle emissions from solid biofuel combustion studied with single-particle mass spectrometry: Identification of markers for organics, soot, and ash components, Journal of Geophysical Research: Atmospheres, 118, 859-870, https://doi.org/10.1029/2012JD018389, 2013.

Pettersson, E., Boman, C., Westerholm, R., Boström, D., and Nordin, A.: Stove Performance and Emission Characteristics in Residential Wood Log and Pellet Combustion, Part 2: Wood Stove, Energy & Fuels, 25, 315-323, 10.1021/ef1007787, 2011.

Pieber, S. M., El Haddad, I., Slowik, J. G., Canagaratna, M. R., Jayne, J. T., Platt, S. M., Bozzetti, C., Daellenbach, K. R., Fröhlich, R., Vlachou, A., Klein, F., Dommen, J., Miljevic, B., Jiménez, J. L., Worsnop, D. R., Baltensperger, U., and Prévôt, A. S. H.: Inorganic Salt Interference on CO2+ in Aerodyne AMS and ACSM Organic Aerosol Composition Studies, Environmental Science & Technology, 50, 10494-10503, 10.1021/acs.est.6b01035, 2016.

Pratsinis, S. E.: Simultaneous nucleation, condensation, and coagulation in aerosol reactors, Journal of Colloid and Interface Science, 124, 416-427, https://doi.org/10.1016/0021-9797(88)90180-4, 1988.

Reavell, K., Hands, T., and Collings, N.: A Fast Response Particulate Spectrometer for Combustion Aerosols, SAE Transactions, 111, 1338-1344, 2002.

Schraufnagel, D. E.: The health effects of ultrafine particles, Experimental & Molecular Medicine, 52, 311-317, 10.1038/s12276-020-0403-3, 2020.

Schwarz, J. P., Gao, R. S., Fahey, D. W., Thomson, D. S., Watts, L. A., Wilson, J. C., Reeves, J. M., Darbeheshti, M., Baumgardner, D. G., Kok, G. L., Chung, S. H., Schulz, M., Hendricks, J., Lauer, A., Kärcher, B., Slowik, J. G., Rosenlof, K. H., Thompson, T. L., Langford, A. O., Loewenstein, M., and Aikin, K. C.: Single-particle measurements of midlatitude black carbon and light-scattering aerosols from the boundary layer to the lower stratosphere, Journal of Geophysical Research Atmospheres, 111, 10.1029/2006JD007076, 2006.

Seinfeld, J. H. and Pandis, S. N.: Atmospheric chemistry and physics : from air pollution to climate change / John H. Seinfeld, Spyros N. Pandis, Third edition., John Wiley & Sons, Hoboken, New Jersey2016.

Symonds, J. P. R., Reavell, K. S. J., Olfert, J. S., Campbell, B. W., and Swift, S. J.: Diesel soot mass calculation in real-time with a differential mobility spectrometer, Journal of Aerosol Science, 38, 52-68, https://doi.org/10.1016/j.jaerosci.2006.10.001, 2007.

Szopa, S., Naik, V., Adhikary, B., Artaxo, P., Berntsen, T., Collins, W. D., Fuzzi, S., Gallardo, L., Kiendler-Scharr, A., Klimont, Z., Liao, H., Unger, N., and Zanis, P.: Short-Lived Climate Forcers, in: Climate Change 2021: The Physical Science Basis. Contribution of Working Group I to the Sixth Assessment Report of the Intergovernmental Panel on Climate Change, edited by: Masson-Delmotte, V., Zhai, P., Pirani, A., Connors, S. L., Péan, C., Berger, S., Caud, N., Chen, Y., Goldfarb, L., Gomis, M. I., Huang, M., Leitzell, K., Lonnoy, E., Matthews, J. B. R., Maycock, T. K., Waterfield, T., Yelekçi, O., Yu, R., and Zhou, B., Cambridge University Press, Cambridge, United Kingdom and New York, NY, USA, 817-922, 10.1017/9781009157896.008, 2021.

https://doi.org/10.5194/ar-2026-24
Preprint. Discussion started: 30 June 2026

Taylor, J. W., Allan, J. D., Liu, D., Flynn, M., Weber, R., Zhang, X., Lefer, B. L., Grossberg, N., Flynn, J., and Coe, H.: Assessment of the sensitivity of core / shell parameters derived using the single-particle soot photometer to density and refractive index, Atmos. Meas. Tech., 8, 1701-1718, 10.5194/amt-8-1701-2015, 2015.

Ting, Y., Mitchell, E. J. S., Allan, J. D., Liu, D., Spracklen, D. V., Williams, A., Jones, J. M., Lea-Langton, A. R., McFiggans, G., and Coe, H.: Mixing State of Carbonaceous Aerosols of Primary Emissions from "Improved" African Cookstoves, Environmental Science & Technology, 52, 10134-10143, 10.1021/acs.est.8b00456, 2018.

United Nations Economic Commission for Europe, U.: Code of good practice for wood-burning and small combustion installations, United Nations, Geneva, ECE/EB.AIR/150, 2021.

Wang, Y., Liu, F., He, C., Bi, L., Cheng, T., Wang, Z., Zhang, H., Zhang, X., Shi, Z., and Li, W.: Fractal Dimensions and Mixing Structures of Soot Particles during Atmospheric Processing, Environmental Science & Technology Letters, 4, 487-493, 10.1021/acs.estlett.7b00418, 2017.

Waters, L.: Summary results of the domestic wood use survery, Tech. rep., Renewable Energy Statistics, available at: https://www. gov. uk …, 2016.

Weimer, S., Alfarra, M. R., Schreiber, D., Mohr, M., Prévôt, A. S. H., and Baltensperger, U.: Organic aerosol mass spectral signatures from wood-burning emissions: Influence of burning conditions and wood type, Journal of Geophysical Research: Atmospheres, 113, https://doi.org/10.1029/2007JD009309, 2008.

World Health Organisation, W.: World Health Organisation Ambient (outdoor) air pollution, 2022.

Xu, H., Ren, Y. a., Zhang, W., Meng, W., Yun, X., Yu, X., Li, J., Zhang, Y., Shen, G., Ma, J., Li, B., Cheng, H., Wang, X., Wan, Y., and Tao, S.: Updated Global Black Carbon Emissions from 1960 to 2017: Improvements, Trends, and Drivers, Environmental Science & Technology, 55, 7869-7879, 10.1021/acs.est.1c03117, 2021.

Ye, Q., Gu, P., Li, H. Z., Robinson, E. S., Lipsky, E., Kaltsonoudis, C., Lee, A. K. Y., Apte, J. S., Robinson, A. L., Sullivan, R. C., Presto, A. A., and Donahue, N. M.: Spatial Variability of Sources and Mixing State of Atmospheric Particles in a Metropolitan Area, Environmental Science & Technology, 52, 6807-6815, 10.1021/acs.est.8b01011, 2018.

Yu, C., Liu, D., Broda, K., Joshi, R., Olfert, J., Sun, Y., Fu, P., Coe, H., and Allan, J. D.: Characterising mass-resolved mixing state of black carbon in Beijing using a morphology-independent measurement method, Atmos. Chem. Phys., 20, 3645-3661, 10.5194/acp-20-3645-2020, 2020.

Zhang, Y., Albinet, A., Petit, J.-E., Jacob, V., Chevrier, F., Gille, G., Pontet, S., Chrétien, E., Dominik-Sègue, M., Levigoureux, G., Močnik, G., Gros, V., Jaffrezo, J.-L., and Favez, O.: Substantial brown carbon emissions from wintertime residential wood burning over France, Science of The Total Environment, 743, 140752, https://doi.org/10.1016/j.scitotenv.2020.140752, 2020.